ANNALS OF PHYSICS 236, 1–42 (1994)

Resonant Tunneling with an Electron–Phonon Interaction

PER HYLDGAARD, SELMAN HERSHFIELD,* JOHN H. DAVIES,†
AND JOHN W. WILKINS

Department of Physics, 174 West 18th Avenue,
Ohio State University, Columbus, Ohio 43210

Received October 12, 1993; revised January 28, 1994

Using nonequilibrium quantum-statistical mechanics, we study both the equilibrium behavior and the nonlinear transport in a one-dimensional model of resonant tunneling with an electron–phonon interaction at zero temperature. There are several unique features of our work: (1) We demonstrate the importance of the Hartree-like electron–phonon self-energy diagram in this problem lacking translational invariance. (2) We identify a new perturbation parameter in the study of the equilibrium polaron shift. (3) We provide a thorough understanding of when the noninteracting current is a poor predictor of the interacting current–voltage characteristic, which we calculate and explain in detail. Our calculation treats a weak electron–phonon interaction at zero temperature perturbatively in the dimensionless coupling constant, g, to lowest self-consistent order. Because the system is not translational invariant, we must retain both a Fock-like *and* a Hartree-like diagram. Depending of the filling condition of the resonant level, the model can be in two qualitatively different regimes: when the resonant level is empty (occupied), the polaron shift of the level with the interaction is $-g\Omega$ ($-3g\Omega$), where Ω is the frequency of the phonon. The crossover occurs on a scale set by the noninteracting escape rate, Γ, and we find that $g\Omega/\Gamma$ is an additional perturbation parameter in the study of the equilibrium polaron shift. We furthermore evaluate typical nonlinear current–voltage characteristics. When the Fermi seas of the leads are much thicker than Ω (and Γ), the interaction affects the total current only near the onset of the large resonant current and in the valley region. However, the interaction modifies the I-V characteristics at all biases when the Fermi seas are shallow. To interpret our results we separate the current densities per unit energy for the left and right leads into elastic and inelastic contributions. We finally show that the qualitative behavior of the inelastic current contributions does not depend on the filling condition of the resonant level for a system with thick Fermi seas at a typical bias where a large current flows.

I. INTRODUCTION

I.A. *Background*

The problem of quantum transport in small semiconductor heterostructures has received considerable attention, both because of its potential technological applications and because quantum mechanics is instrumental to understanding the electron

* Present address: Department of Physics, University of Florida, Gainesville FL 32611.
† Permanent address: Department of Electronics and Electrical Engineering, Glasgow University, Glasgow G12 8QQ, UK.

0003-4916/94 $9.00

transport. The original theoretical work focused on noninteracting electrons in the linear response regime [1, 2]. As progress has been made in the understanding of noninteracting electron transport, theoretical work has increasingly turned to transport in the presence of many-body interactions such as the electron–phonon interaction; see, for example, Refs. [3–13]. Since it is easy to drive small heterostructures far out of equilibrium, a study of the nonlinear response regime is often needed to compare with experiments. There has therefore been a growing theoretical interest in nonequilibrium transport [14–35].

In this paper we consider the problem of resonant tunneling with an electron–phonon interaction, as a particular example of transport in a nonequilibrium, interacting quantum system. We study a one-dimensional model and our calculations describe qualitatively the resonant tunneling with an electron–phonon interaction observed in Refs. [36, 37]. Our calculations does not allow a quantitative comparison with these experiments performed on a standard double-barrier semiconductor heterostructures because: (1) We do not allow the electrons to move in directions that are perpendicular to the current flow. (2) We do not include the charging effects on the double-barrier potential produced in the semiconductor heterostructure. While our formal calculations could easily be generalized to three dimensions to address (1), the numerical evaluations would be much more involved and we have not attempted to obtain such a quantitative description. Instead we hope our one-dimensional model calculations serve to illustrate some qualitative features of resonant tunneling with an electron–phonon interaction.

In particular, our calculation is relevant for resonant tunneling through localized states; see Refs. [38–41]. These experiments show both a Coulomb blockade at low biases (and low temperatures) and evidence of electron–phonon interactions at higher biases. Our model does not include the electron–electron interaction needed to model the Coulomb blockade at a low bias. However, we believe that our nonequilibrium calculation can be used to gain qualitative understanding of resonant tunneling through such localized states at higher biases (where the Coulomb blockade can be neglected). In this sense previous studies [17, 18, 23, 25, 30, 34] of electron–electron interaction in resonant tunneling through a localized state (Anderson impurity) here are supplemented by a study of the inelastic effects of the electron–phonon interaction.

A standard semiconductor heterostructure realization of a resonant tunneling device comprises (for example) an n-doped GaAs lead, a double-barrier region, and finally another n-doped GaAs lead. The double-barrier region consists of an undoped AlGaAs barrier, an undoped GaAs central region, followed by a second undoped AlGaAs barrier. Current flows through these alternating AlGaAs and GaAs layers in the presence of an applied bias. The electron motion in the current direction is determined by a double-barrier potential similar to the potential shown in Fig. 1. This double-barrier potential traps a resonant level of energy E_r in the central GaAs region and this resonant level can result in a significantly enhanced tunneling current.

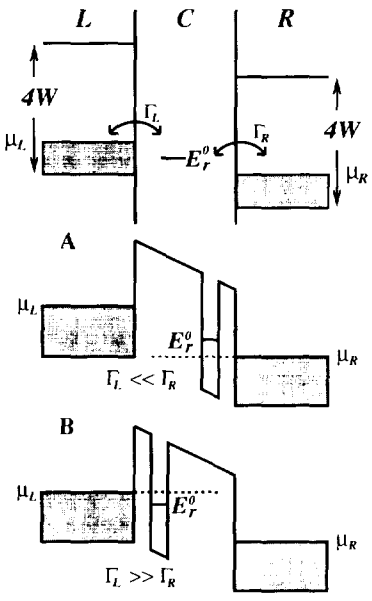

FIG. 1. Schematic of resonant tunneling through a level with an electron–optical phonon interaction (upper panel) and two different qualitative regimes **A** (middle panel) and **B** (lower panel). In regime **A** (showing a small negative polaron shift and a satellite peak in resonant-site density of states $N(\omega) = -\mathrm{Im}\, g_r(\omega)/\pi$ *above* main peak at E_r) the interacting resonant level can be treated as empty, whereas in regime **B** (showing a larger negative polaron shift and a satellite peak in density of state *below* main peak) the interacting resonant level must be treated as occupied. Consider the schematic of the model (upper panel). The left and right leads are described by one-dimensional tight-binding models with a bandwidth of $4W$. In equilibrium μ is the chemical potential in both leads. At a finite bias V the left (right) lead have chemical potential $\mu_{L(R)} = \mu + (-)eV/2$, and the lower band-edge is at $\phi_{L(R)} = -2W + (-)e^{V/2}$. The escape rate Γ_L (Γ_R) connects the central resonant site to the left (right) lead, giving a non-interacting resonant level E_r^0. The interaction (via matrix element M) at the central site only with a single phonon mode (of frequency Ω) renormalizes the resonant level to E_r. In equilibrium, regime **A** (**B**) obtains when $E_r - \mu \gg \Gamma_L + \Gamma_R$ ($\mu - E_r \gg \Gamma_L + \Gamma_R$). Equally important, as illustrated in the middle (lower) panel, the chemical potential for the lead most strongly connected to the resonant level (μ_R (μ_L) in middle (lower) panel) sets the filling condition of the central site: $E_r \gg \mu_R$ ($E_r \ll \mu_L$) is empty (occupied) in the middle (lower) panel. Thus regime **A** (**B**) also is obtained at a typical finite bias when $\Gamma_L \ll \Gamma_R$ ($\Gamma_L \gg \Gamma_R$).

Consider a resonant level which in equilibrium is located above the chemical potential of the leads. As illustrated in Fig. 1, an applied bias raises both the chemical potential and the conduction-band energies of the left lead, relative to the resonant level, while lowering the chemical potential and energies in the right lead. The following simple picture of resonant tunneling therefore presents itself in the absence of interactions. Because electrons will tunnel almost exclusively when their energy is at E_r, the linear response conductivity is typically small. However, when a finite bias pushes the chemical potential of the left lead above E_r, there is a

dramatic increase in the current. The region of the current-voltage (I-V) characteristic with large resonant currents persists until the bias pushes the lower band-edge of the left lead above E_r. The resonant level is then no longer available for electrons in the left lead and only a small current flows in the so-called valley region of the I-V characteristic. When the system enters this valley region the current *decreases* with increasing applied bias, resulting in a region of negative differential conductance, $dI/dV < 0$. This feature has potential applications in devices designed to operate at very high frequencies and has motivated a sustained interest in resonant tunneling since its first observation in 1974 [44].

In addition to the interest devoted to resonant tunneling in the standard double-barrier heterostructure, there have been several recent measurements of resonant tunneling through localized states [38–41] and of the current tunneling through a narrow metal point contact containing disorder [42, 43]. The experiments reported in Refs. [38–40] considered transport through thin amorphous Si/SiO_x tunnel structures. Tunneling across the SiO_x barriers can occur either directly or via impurity states (forming the resonant levels) in the SiO_x barrier. In the experiment reported in Ref. [41], resonant tunneling occurs between two gold wires via intermediate atoms. Because the resonant tunneling occur via *localized* states in Refs. [38–41], the electrons are restricted in these experiments to move only in the direction of the current. This restriction of the electron motion perpendicular to the current flow separates the resonant tunneling in Refs. [38–41] from the resonant tunneling in the standard double-barrier heterostructures where the electrons are free to move in the two perpendicular directions. The distinction is irrelevant in the absence of interactions and impurity scattering: The double-barrier potential with resonant level E_r shown in Fig. 1 fully describes the noninteracting resonant tunneling through localized states as well as the noninteracting resonant tunneling in the standard semiconductor heterostructure. However, the difference is important when one considers resonant tunneling in the presence of impurity scattering because of the potential momentum transfer between the directions parallel and perpendicular to the current [19, 20]. Similarly, interacting resonant tunneling in the standard three-dimensional double-barrier heterostructure must in principle also be studied within a three-dimensional model as in Refs. [13, 35]. In contrast, interacting resonant tunneling through a localized state remains a one-dimensional problem.

A study of tunneling in the presence of interactions is well motivated both for the standard double-barrier semiconductor heterostructures and for the measurements of resonant tunneling through localized states. The coupling to optical phonons is strong in GaAs and AlGaAs semiconductors, and there is direct experimental evidence for electron–phonon interactions in the standard double-barrier heterostructure: A current shoulder observed in the valley region is attributed to electrons which emit an optical phonon while tunneling [36, 37].

Inelastic scattering is also important when treating resonant tunneling through localized states [38–41]. In the experiment reported in Ref. [41] the tunneling between two gold wires via intermediate atoms shows not only a Coulomb

blockade effect at low biases, but also at higher biases the vibrational modes of these atoms. In the experiments reported in Refs. [38–40] the resonant tunneling was suppressed at low biases, and this suppression has been interpreted as a Coulomb blockade effect [39]. At a large bias, however, transport occurs as tunneling through a single impurity state (resonant tunneling) or at still higher biases as tunneling through a sequence of states (hopping) [40]. This hopping regime is possible because electron–phonon scattering allows the tunneling electron to make transitions between localized states of different energy [6]. As in Ref. [41], the tunneling experiments reported in Refs. [38–40] therefore show evidence of a Coulomb blockade effect at low biases and of an electron–phonon interaction at larger biases. Thus, transport in resonant tunneling systems must in general be understood in the presence of inelastic scattering and, in particular, the electron–phonon scattering.

As stated above, here we consider the problem of resonant tunneling with an electron–phonon interaction within a one-dimensional model. We have not attempted to provide a quantitative description of the interacting resonant tunneling in the standard double-barrier heterostructure (which would require a study of a three-dimensional model). Instead we hope that our one-dimensional model calculations serve to illustrate qualitative features of resonant tunneling with an electron–phonon interaction by studying both the equilibrium and the non-equilibrium transport at zero temperature. In addition to qualitatively describing resonant tunneling with an electron–phonon interaction in the standard double-barrier heterostructures, our calculations are relevant for experiments on interacting resonant tunneling through localized states; see Refs. [38–41].

Glazman and Shekhter [4] and Wingreen *et al* [5] gained a qualitative understanding of resonant tunneling with an electron–phonon interaction by evaluating the single-electron transmission coefficient, $T_{\rm tot}(\omega)$, which is the probability for tunneling of an electron with incoming energy ω. Consider the case of electrons interacting with a single optical mode of frequency Ω at zero temperature. The transmission coefficient, $T_{\rm tot}(\omega)$, then has a main peak at the resonant level, E_r, and satellite peaks at $E_r+\Omega$, $E_r+2\Omega$, ... The satellite peak in the transmission probability at $E_r+\Omega$ corresponds to electrons which enter the resonant level at $E_r+\Omega$, but which decay via a phonon-emission process into the resonant level. When the resonant tunneling system is in the valley region and the lower band-edge of the left lead is above the resonant level, these inelastic tunneling processes result in an increased tunneling probability compared to the noninteracting case. This explains the experimentally observed shoulder in the current [36, 37, 5].

An explanation of the current shoulder based on a single-electron treatment is justified because the shoulder occurs in the valley region where: (1) The applied bias is large enough that the electrons of the right lead can be ignored. (2) The filling condition of the resonant level is empty, and the tunneling of any one electron is not influenced by other electrons at the resonant level. However, the single-electron treatment is not valid under general conditions. For example, if the

applied bias is less than the characteristic phonon-frequency, then electrons in the right lead will inhibit the decay of the tunneling electron via phonon emission due to the Pauli exclusion principle. Also, if we permit electrons of both spins to occupy the resonant level, the electron–phonon interaction can mediate an effective electron–electron interaction between the electrons of opposite spin at the resonant level; see Section I.C below.

To describe resonant tunneling with an electron–phonon interaction under general filling conditions one must leave the single-electron description. In this paper we apply nonequilibrium quantum-statistical mechanics [45–47] to the one-dimensional model of a resonant tunneling system, consisting of left and right leads without any interactions, and a central resonant level, where electrons interact with a single phonon mode of frequency Ω. We follow a procedure first introduced by Caroli *et al.* [14] and do perturbation simultaneously in the electron–phonon interaction and in a tunneling term connecting the resonant level to the two leads. An advantage of this approach is that it is only necessary to calculate the Green functions self-consistently at the resonant level, making the numerical calculations simple. Because the electron–phonon interaction is assumed to be small, we treat the interaction in the self-consistent Born approximation, where only the lowest order self-energies are kept.

This paper is an outgrowth of a study of Hershfield *et al.* [25, 30] on resonant tunneling through an Anderson impurity. Our paper is similar to the recent calculation by Anda and Flores [24] of resonant tunneling with an electron–phonon interaction. However, although both papers use nonequilibrium quantum-statistical mechanics within the self-consistent Born approximation, there are some differences between our work and that of Ref. [24]. The self-energies were evaluated also at a finite temperature in Ref. [24], while we study the model at zero temperature only. We have furthermore restricted the interaction to the resonant site, while in Ref. [24] the interaction was also extended to a finite central region. On the other hand, we find it essential to include a Hartree-like electron–phonon diagram in this system that is lacking translational invariance [48]. Only then do we obtain the correct polaron shift in the limit where the resonant level is occupied. The self-consistent Born approximation treats the interaction to lowest order in the obvious perturbation parameter, $g \equiv M^2/\Omega^2$, where M denotes the electron–phonon matrix element. However, for some properties, such as the equilibrium polaron shift at zero temperature, we find that there is an additional perturbation parameter, $g\Omega/\Gamma$, where Γ is the (noninteracting) escape rate from the resonant level. This second perturbation parameter is important in the physically relevant case that the optical mode frequency is greater than the escape rate, $\Omega/\Gamma > 1$.

The current can be approximated by an integral of a function $T_a(\omega)$, from the chemical potential of the right lead, μ_R, to the chemical potential of the left lead, μ_L. When the escape rates for tunneling of the resonant level to either lead are constant this approximation is exact. There is, however, a correction term when the escape rates depend on the energy [25, 28, 30, 32]. We demonstrate that for the case of resonant tunneling with an electron–phonon interaction this correction can

become significant in the valley region. We also find that $T_a(\omega)$ does not describe the current density per unit energy at the resonant level, even when the escape rates are constant, and it is not possible to interpret $T_a(\omega)$ as an effective transmission coefficient for the interacting problem. Instead we consider the current densities for the left and right leads. By separating these current densities into elastic and inelastic contributions based on the principles discussed in an earlier paper [32], we can follow the transfer of energy at the resonant level from the electrons to the phonon system. We finally show that the qualitative form of the inelastic current contributions does not depend on the filling condition of the resonant level, for a typical tunneling system at a bias where a large resonant current flows.

A problem with our calculation is that the interaction is restricted to the resonant level only. There is no scattering in the barriers or in the leads. A recent study [35] included electron–phonon interactions in the barriers, and scattering was included everywhere in two other recent calculations [22, 26]. A complete quantitative description of resonant tunneling must include scattering everywhere, but omitting the interaction with *optical* phonon modes in the leads is a reasonable approximation here because the emission of optical phonons is only important in regions with a finite potential drop, and the emission processes are therefore limited to the double-barrier region and surrounding areas. In our model we assume that voltage drop occurs exclusively across the two barriers, and we restrict the interaction to the central resonant level, neglecting the weaker interaction in the barriers.

The rest of this paper is organized as follows. In the next two subsections we introduce the model and identify its qualitatively different regimes. In Section II we define the nonequilibrium Green functions and evaluate them numerically in the self-consistent Born approximation and analytically in the first Born approximation. The equilibrium interacting density of states is calculated in different regimes, and we identify an additional perturbation parameter by studying the equilibrium polaron shift. We also discuss the exact position of the satellite peak in the density of state. In Section III we verify that current is conserved and report the calculations of the nonlinear I-V characteristics. We evaluate the current density per unit energy at the resonant site and for the left and right leads. We finally separate the current densities for the left and right leads into elastic and inelastic contributions. The results are summarized in Section IV.

I.B. *Model Hamiltonian*

The model Hamiltonian has four terms: H_d, describing the disconnected two leads and noninteracting central resonant level; H_T, the tunneling processes; H_{ph}, the optical phonon and H_{ep}, its interaction with electrons. A schematic of the resonant tunneling model is shown in the upper panel of Fig. 1. The Hamiltonian H_d models the three disconnected subsystems: the left lead (L), the right lead (R), and a central resonant level (C). The left lead (sites $j \leqslant -1$) and the right lead ($j \geqslant 1$) are described by one-dimensional tight-binding models of bandwidth $4W$ and

site-energies E_L and E_R, respectively. The single central resonant state (at $j=0$) have site energy E_C. Thus

$$\begin{aligned} H_d = &- W \sum_{j \leqslant -1,s} (c^+_{j-1,s} c_{j,s} + c^+_{j,s} c_{j-1,s}) + E_L \sum_{j \leqslant -1,s} c^+_{j,s} c_{j,s} \\ &- W \sum_{j \geqslant 1,s} (c^+_{j+1,s} c_{j,s} + c^+_{j,s} c_{j+1,s}) + E_R \sum_{j \geqslant 1,s} c^+_{j,s} c_{j,s} \\ &+ E_C \sum_s c^+_{0,s} c_{0,s}, \end{aligned} \tag{1}$$

where the spin index s is summed over $s = \uparrow, \downarrow$. A tunneling term,

$$H_T = -W_L \sum_s (c^+_{0,s} c_{-1,s} + c^+_{-1,s} c_{0,s}) - W_R \sum_s (c^+_{1,s} c_{0,s} + c^+_{0,s} c_{1,s}), \tag{2}$$

links the central region C to the left/right lead with escape rate $\Gamma_{L/R}$ and renormalizes the isolated site energy E_C to the noninteracting resonant level E_r^0 [49]. Finally there is an optical phonon mode (b) of energy Ω, which interacts with electrons at the resonant site

$$H_{ph} = \Omega b^+ b, \tag{3}$$

$$H_{ep} = M(c^+_{0,\uparrow} c_{0,\uparrow} + c^+_{0,\downarrow} c_{0,\downarrow})(b^+ + b). \tag{4}$$

The dimensionless coupling constant $g \equiv (M^2/\Omega^2)$ is set to 0.1 in this paper.

When the three regions are disconnected, the left (right) lead is in equilibrium at chemical potential $\mu_{L(R)}$ and hence is described by the Fermi distribution function

$$f_{L(R)}(\omega) = \frac{1}{e^{\beta(\omega - \mu_{L(R)})} + 1}, \tag{5}$$

where $1/\beta$ is the temperature. The difference in the chemical potentials μ_L and μ_R is set by the applied bias $eV = \mu_L - \mu_R$. The common equilibrium chemical potential is denoted μ. For equal carrier-densities in the left and right leads, we have

$$\mu_L - E_L = \mu_R - E_R, \tag{6}$$

and we choose the zero point of the energy so that $E_L = E_R = 0$ in equilibrium. Assuming that the voltage drop occurs symmetrically we then have $E_{L(R)} = +(-)eV/2$, and $\mu_{L(R)} = \mu + (-)eV/2$. We denote the lower band-edge of the left (right) lead by $\phi_{L(R)} = +(-)eV/2 - 2W$. Table I summarizes the model parameters and the specific choice of these parameters in the perturbation calculations reported in Sections II and III.

I.C. *Regimes of the Model*

The density of states or the spectral function at the interacting central site for spin s is defined

$$N_s(\omega) \equiv \frac{1}{2\pi} \int d(t-t')\, e^{i\omega(t-t')} \langle \{c^+_{0,s}(t'), c_{0,s}(t)\} \rangle. \tag{7}$$

TABLE I

Model Parameters Used in the Equilibrium Study and in the Calculation of the Nonlinear Transport

Physical quantity	Symbol	Equilibrium study, high-doping (Figs. 3, 4, 5)	I-V characteristic, high-doping (Figs. 6, 8, 9)	I-V characeristic, low-doping (Fig. 7)
Bandwith of left/right lead	—	$4W$	$4W$	$4W$
Tunnel matrix elements in H_T	$W_L = W_R$	$0.1W$	$0.1W$	$0.15W$
Isolated resonance level	E_C	0	$-0.7W$	$-1.1W$
Noninteracting resonance level	E_r^0	0	$-0.71W$	$-1.13W$
Equilibrium chemical potential	μ	$-0.16W$ to $0.08W$	$-0.9W$	$-1.5W$
Phonon frequency	Ω	$0.2W$	$0.2W$	$0.7W$
Band-with in fixed Ω	$4W$	20Ω	20Ω	$5.7W$
Depth of equilibrium Fermi sea	$\mu + 2W$	$\approx 10\Omega$	5.5Ω	0.7Ω

Note. The unit energy is the overlap-integral W of the tight-binding model for the two leads. In the study of the equilibrium resonant-site density of states, of the equilibrium polaron shift and of the position of the satellite peaks [see Figs. 3–5], we consider a high-doping (and wide-band) situation, where the varying depth of the equilibrium Fermi sea, $\mu + 2W$ (and the bandwidth of the leads, $4W$), is large compared to the phonon frequency Ω. The same high-doping situation is considered in the I-V characteristic shown in Fig. 6. In the nonequilibrium calculations at the finite applied bias V, the left (right) lead have site-energy $E_{L(R)} = +(-)eV/2$ and chemical potential $\mu_{L(R)} = \mu + (-)eV/2$, where μ is the corresponding equilibrium ($V = 0$) chemical potential. Figure 6 shows the I-V characteristic for the high-doping situation with $\mu + 2W = 5.5\Omega$. We also calculate a low-doping I-V characteristic shown in Fig. 7, where the depth of the (corresponding) equilibrium Fermi sea, $\mu + 2W$, is comparable to Ω, and where the bandwidth, $4W$, is reduced to approximately 6Ω. In Fig. 6 the high-doping system has $W_L^2/W = W_R^2/W = 0.05\Omega$, but in Fig. 8 we compare that situation to one where $W_L^2/W = 0.01\Omega$ and $W_R^2/W = 0.09\Omega$ (while maintaining the other parameters). In Fig. 9 the high-doping situation with $W_L \ll W_R$ is investigated further. The values of the noninteracting resonant level E_r^0 applies when E_r^0 is still within both bands and when $W_L = W_R$; see Ref. [49]). We assume that the temperature is zero ($1/\beta = 0$) and that the dimensionless coupling constant, $g \approx M^2/\Omega^2$, is set to $g = 0.1$. At a finite bias V the lower band-edge of the left (right) lead is given by $\phi_{L(R)} = +(-)eV/2 - 2W$.

The shape of the resonant-site density of states determines the qualitative behavior of the model. The noninteracting density of states has a single peak at E_r^0 (the noninteracting resonant level). In the interacting system, the density of states has a main peak at E_r (the interacting resonant level), but it also has additional satellite peaks.

We find two different regimes **A** and **B** of the interacting system, depending on the filling condition of the resonant level. In regime **A** the interaction shifts the resonant level to $E_r = E_r^0 - g\Omega$ and the density of states acquires a satellite peak situated approximately Ω *above* the main peak at E_r. In regime **B** the resonant level is shifted to $E_r = E_r^0 - 3g\Omega$, and the density of states has a satellite peak approximately Ω *below* E_r. Regime **A** occurs when the resonant level is empty ($\mu \ll E_r$), while **B** occurs when the resonant level is occupied ($\mu \gg E_r$). Equally important, as illustrated in Fig. 1, both regime **A** and regime **B** also are obtained at a typical finite bias, with a large current flowing through the resonant tunneling system. The resonant level E_r is then above μ_R (and above ϕ_L), but below μ_L. If in this situation $\Gamma_L \ll \Gamma_R$ then the resonant level is mostly empty (regime **A**), but if $\Gamma_L \gg \Gamma_R$ the resonant level is mostly occupied (regime **B**).

We refer, by the phrase polaron shift, to the small (large) negative shift of the resonant level in regime **A** (**B**). In the polaron problem the energy of a single electron is shifted with the electron–phonon interaction. Here, because the two regimes have different filling conditions, different polaron shifts are observed. Consider the isolated central site in the presence of an electron–phonon interaction within second-order perturbation theory. The model Hamiltonian is

$$H_i = E_C \sum_s c_{0,s}^+ c_{0,s} + \Omega b^+ b + M(c_{0,\uparrow}^+ c_{0,\uparrow} + c_{0,\downarrow}^+ c_{0,\downarrow})(b^+ + b). \tag{8}$$

Let E_n be the energy of having $n = 0, 1, 2$ electrons at the level. These energies are to second order in M,

$$\begin{aligned} E_0 &= 0, \\ E_1 - E_C &= \frac{M^2}{E_C - (E_C + \Omega)} = -g\Omega, \\ E_2 - 2E_C &= \frac{(M+M)^2}{2E_C - (2E_C + \Omega)} = -4g\Omega, \end{aligned} \tag{9}$$

where we have used $g \equiv (M^2/\Omega^2)$. For E_2 the matrix element between the intermediate state (with a single phonon) and the unperturbed ground state obtains a contribution from both spins in the interaction term of Hamiltonian H_i (Eq. (8)). In regime **A**, where the level is empty, the expectation value in Eq. (7) reduces to

$$\langle \{c_{0,s}^+(t'), c_{0,s}(t)\} \rangle = e^{-i(E_1 - E_0)(t - t')}, \tag{10}$$

while in regime **B**, where the level is (doubly) occupied, it reduces to

$$\langle \{c_{0,s}^+(t'), c_{0,s}(t)\} \rangle = e^{-i(E_2 - E_1)(t - t')}. \tag{11}$$

Without loss of generality we can put $E_C = 0$, and within second-order perturbation theory, we therefore find a *small* negative polaron shift of $E_1 - E_0 = -g\Omega$ in regime **A**, but a *large* negative polaron shift of $E_2 - E_1 = -3g\Omega$ in regime **B**.

The difference in the polaron shift is a consequence of the effective electron–electron interaction resulting from the electron–phonon interaction. The canonical transformation [50] $\bar{H}_i \equiv e^S H_i e^{-S}$, where $S = (M/\Omega)(c_\uparrow^+ c_\uparrow + c_\downarrow^+ c_\downarrow)(b^+ - b)$, yields

$$\bar{H}_i = -g\Omega c_{0,\uparrow}^+ c_{0,\uparrow} - g\Omega c_{0,\downarrow}^+ c_{0,\downarrow} - 2g\Omega c_{0,\downarrow}^+ c_{0,\uparrow}^+ c_{0,\uparrow} c_{0,\downarrow} + \Omega b^+ b. \tag{12}$$

Thus, due to the electron–phonon interaction there is an effective *atractive* electron–electron interaction. Subsequently the excitation energy of a particle is smaller than that of a hole, and the polaron shift in regime **A** is smaller than the polaron shift in regime **B**.

II. Interacting Resonant Tunneling in the Born Approximation

In this section we study the nonequilibrium problem of resonant tunneling at zero temperature using perturbation theory. We assume a weak electron–phonon coupling and describe the interaction within the self-consistent Born approximation. We characterize the two regimes **A** and **B** of the model by the polaron shift and by the shape of the interacting, resonant-site density of states or spectral function. By studying the equilibrium, zero-temperature polaron shift, both numerically and analytically within the first Born approximation, we find a new perturbation parameter in the problem, $g\Omega/\Gamma$, where Γ is the escape rate from the resonant level. This parameter is important in the physically relevant case of an optical phonon frequency Ω greater than Γ.

II.A. *Nonequilibrium Green Functions*

To study resonant tunneling we use nonequilibrium quantum-statistical mechanics as introduced by Kadanoff and Baym [45] and by Keldysh [46]. In this approach one starts at some initial time t_0 with an equilibrium system and then turns on a perturbation to drive the system out of equilibrium. Here we start with the equilibrium system of the three *isolated* subsystems contained in H_d. At time $t_0 \to -\infty$, both the tunneling term H_T and the electron–phonon interaction term H_{ep} are adiabatically turned on. If the two leads originally are at a different chemical potentials, this perturbation drives the system out of equilibrium, and a current flows through the resonant level.

Following Langreth [47] we introduce a redundant set of four Green functions with different time-orderings,

$$g_<(j, t, j', t') = \langle c_{j',s'}^+(t')\, c_{j,s}(t)\rangle, \tag{13}$$

$$g_>(j, t, j', t') = \langle c_{j,s}(t)\, c_{j',s'}^+(t')\rangle, \tag{14}$$

$$g_r(j, t, j', t') = -i\Theta(t - t')\langle\{c_{j,s}(t), c_{j',s'}^+(t')\}\rangle, \tag{14}$$

$$g_a(j, t, j', t') = i\Theta(t' - t)\langle\{c_{j,s}(t), c_{j',s'}^+(t')\}\rangle. \tag{14}$$

The brackets indicate a thermal average at $t_0 \to -\infty$. The time-dependent operators $c_{j,s}(t)$ are in the Heisenberg representation. We have omitted the spin index on the Green functions, because they are independent of spin. The four Green functions are related via

$$i(g_r - g_a) = g_< + g_>, \tag{15}$$

$$g_a(j, t, j', t')^* = g_r(j', t', j, t). \tag{16}$$

To evaluate the Green functions we solve the Dyson equations as described in Refs. [25, 30, 32]. Several simplifications are possible in this problem. Since we are interested in the steady state solution of the interacting Hamiltonian, $H = H_d + H_T + H_{ph} + H_{ep}$, all Green functions depend on $(t - t')$ only, and the Dyson equations can be Fourier transformed in time. Furthermore, because the self-energies are restricted to the central resonant site only $(\sigma_{r,<}(j, j'; \omega) \equiv \delta_{j,0}\delta_{j',0}\sigma_{r,<}(\omega))$, the general form of the Green functions can be expressed in terms of the resonant-site Green functions $g_{r,<}(\omega) \equiv g_{r,<}(j = 0, j' = 0; \omega)$.

To simplify the expressions for the Green functions we introduce the scaled energies,

$$\varepsilon_{L/R} = \left(\frac{\omega - E_{L/R}}{2W}\right), \tag{17}$$

and the dimensionless factor,

$$C(\varepsilon) = \begin{cases} -\varepsilon + \sqrt{\varepsilon^2 - 1}, & \text{if } \varepsilon > 1, \\ -\varepsilon + i\sqrt{1 - \varepsilon^2}, & \text{if } |\varepsilon| < 1, \\ -\varepsilon - \sqrt{\varepsilon^2 - 1}, & \text{if } \varepsilon < -1. \end{cases} \tag{18}$$

The escape rates $\Gamma_{L(R)}(\omega)$ for tunneling off the resonant level to the left (right) lead are

$$\Gamma_{L(R)}(\omega) = \Theta(1 - |\varepsilon_{L(R)}|) \frac{W_{L(R)}^2}{W} \sqrt{1 - \varepsilon_{L(R)}^2}. \tag{19}$$

Note that the escape rate for going to the left (right) lead vanishes when the energy ω approaches the lower band-edge of the left (right) lead, $\phi_{L(R)}$. The resonant-sites retarded and less-than Green functions are [25, 30]

$$g_r(\omega) = \frac{1}{\omega - E_C + (W_L^2/W)\, C(\varepsilon_L) + (W_R^2/W)\, C(\varepsilon_R) - \sigma_r(\omega)}, \tag{20}$$

$$g_<(\omega) = |g_r(\omega)|^2 \left[2f_L(\omega)\, \Gamma_L(\omega) + 2f_R(\omega)\, \Gamma_R(\omega) + \sigma_<(\omega)\right]. \tag{21}$$

The resonant-site density of states or spectral function is related to the retarded Green function by

$$2\pi N(\omega) = -2 \operatorname{Im} g_r(\omega) = |g_r(\omega)|^2 \left[2\Gamma_L(\omega) + 2\Gamma_R(\omega) - 2 \operatorname{Im} \sigma_r(\omega)\right], \tag{22}$$

TABLE II

The Resonant-Site Green Functions and the Zero-Temperature Self-Energies in the Self-Consistent Born Approximation

Resonant-site Green function:

$$(g_r(\omega))^{-1} = \omega - E_C + (W_L^2/W)\, C(\varepsilon_L) + (W_R^2/W)\, C(\varepsilon_R) - \sigma_r(\omega),$$

$$g_<(\omega) = |g_r(\omega)|^2\, [2f_L(\omega)\, \Gamma_L(\omega) + 2f_R(\omega)\, \Gamma_R(\omega) + \sigma_<(\omega)].$$

Self-energies:

$$\frac{\sigma_r(\omega)}{M^2} = -4 \int \frac{d\omega'}{2\pi} \frac{g_<(\omega')}{\Omega} + P \int \frac{d\omega'}{2\pi} \left(\frac{g_>(\omega' - \Omega) + g_<(\omega' + \Omega)}{\omega - \omega'} \right) - i \frac{1}{2} (g_>(\omega - \Omega) + g_<(\omega + \Omega)),$$

$$\frac{\sigma_<(\omega)}{M^2} = g_<(\omega + \Omega).$$

Using:

$$\varepsilon_{L/R} = \left(\frac{\omega - E_{L/R}}{2W} \right),$$

$$C(\varepsilon) = \begin{cases} [-\varepsilon + \sqrt{\varepsilon^2 - 1}], & \text{if } \varepsilon > 1, \\ [-\varepsilon + i\sqrt{1 - \varepsilon^2}], & \text{if } |\varepsilon| < 1, \\ [-\varepsilon - \sqrt{\varepsilon^2 - 1}], & \text{if } \varepsilon < -1. \end{cases} \qquad \Gamma_{L/R}(\omega) = \Theta(1 - |\varepsilon_{L/R}|) \frac{W_{L/R}^2}{W} \sqrt{1 - \varepsilon_{L/R}^2},$$

$$f_{L/R}(\omega) = \frac{1}{e^{\beta(\omega - \mu_{L,R})} + 1}.$$

Note. The four functions $g_r(\omega)$, $g_<(\omega)$, $\sigma_r(\omega)$, and $\sigma_<(\omega)$ are solved for simultaneously (using $g_>(\omega) \equiv -2 \operatorname{Im} g_r(\omega) - g_<(\omega)$). The first energy-independent term in $\operatorname{Re} \sigma_r(\omega)$ is the contribution from the Hartree diagram shown in Fig. 2a. It is essential in describing correctly the polaron shift in regime **B**, where the resonant level is completely occupied.

where we have, of course, dropped the spin subscript on the density of states. In Table II we summarize the results for the interacting resonant-site Green functions. The noninteracting Green functions $g_r^0(\omega)$ and $g_<^0(\omega)$, corresponding to Hamiltonian $H_0 = H_d + H_T$, are obtained from Eqs. (20) and (21) by setting $\sigma_r(\omega) = \sigma_<(\omega) = 0$.

The self-energies $\sigma_r(\omega)$ and $\sigma_<(\omega)$ in Eqs. (20) and (21) are expressed in terms of the electron and phonon Green functions. The Green functions of the (free) phonon mode b (living only at the central site) are defined

$$d_<(t-t') = -\langle (b(t') + b^+(t'))(b(t) + b^+(t)) \rangle, \tag{23}$$

$$d_>(t-t') = \langle (b(t) + b^+(t))(b(t') + b^+(t')) \rangle, \tag{24}$$

$$d_r(t-t') = -i\Theta(t-t')\langle [(b(t) + b^+(t)), (b(t') + b^+(t'))] \rangle, \tag{25}$$

$$d_a(t-t') = i\Theta(t'-t)\langle [(b(t) + b^+(t)), (b(t') + b^+(t'))] \rangle. \tag{26}$$

The free phonon mode is assumed to remain in equilibrium despite the interaction and to be described by the Bose–Einstein distribution function

$$f_B(\Omega) = \frac{1}{e^{\beta\Omega} - 1}. \tag{27}$$

The energy of an optical phonon is large, compared with typical experimental temperature, $\beta\Omega \gg 1$. We have, furthermore, chosen to study the model in the limit where the temperature is small, not only compared to Ω but also on an energy-scale set by the escape rates $\Gamma_{L/R}(\omega)$. We therefore evaluate the Green functions and self-energies at zero temperature ($1/\beta \equiv 0$).

II.B. *The Self-Consistent Born Approximation*

In this paper we assume that the electron–phonon interaction is small, i.e., $g = 0.1$. In a perturbative approach it is then necessary to keep only the lowest-

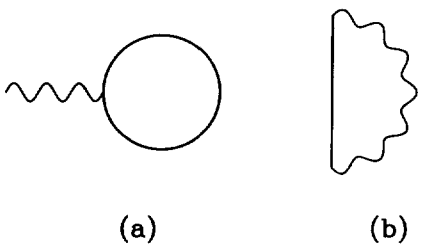

FIG. 2. The self-energy diagrams for the (self-consistent) Born approximation, which consist of the diagrams to lowest order in the dimensionless coupling constant g. The wavy lines represent free phonon Green functions. The straight lines represent either the noninteracting or the interacting electron Green functions, corresponding to either the first or the self-consistent Born approximation, respectively. In this problem lacking translational invariance, both the Hartree-like diagram (panel **a**) and the Fock-like diagram (panel **b**) must be retained. In the study of the polaron shift we found the Hartree diagram essential to correctly describe the behavior in regime **B**, where the resonant level is occupied.

order diagrams. Figure 2 shows the two first-order diagrams in $g \equiv (M^2/\Omega^2)$. We refer to the diagram in Fig. 2a as the the Hartree diagram and to the diagram in Fig. 2b as the Fock diagram, by analogy to the treatment of the electron–electron interaction [51]. In order to construct a current-conserving approximation [52] the self-energy diagrams are evaluated using self-consistent expressions for the electron Green functions. Because the system lacks translational invariance [48], it is essential to retain the Hartree diagram to correctly describe the model in regime **B**.

We denote the self-consistent approximation, based on the diagrams of Fig. 2, the self-consistent Born approximation. The contribution $\sigma^{(H)}$ from the Hartree diagram is independent of time,

$$\begin{aligned} \sigma^{(H)} &= n_s M^2 g_<(0, t=0, 0, t'=0)\, d_r(\omega=0) \\ &= -2n_s \frac{M^2}{\Omega} \int \frac{d\omega'}{2\pi}\, g_<(\omega'), \end{aligned} \tag{28}$$

where $d_r(\omega'=0) = -2/\Omega$ is the integral of the retarded phonon Green function (see Eq. (25)) and where the spin-degeneracy is $n_s = 2$. The effect of the Hartree diagram is therefore similar to that of an (electron density-dependent) single-particle potential and can formally be described as an energy-independent contribution to the real part of the self-energy:

$$\sigma_r^{(H)} = -4 \frac{M^2}{\Omega} \int \frac{d\omega'}{2\pi}\, g_<(\omega'), \qquad \sigma_{<,>}^{(H)} = 0. \tag{29}$$

Hence, the Hartree and Fock diagrams yield at zero temperature

$$\sigma_{\lessgtr}(\omega) = M^2 g_{\lessgtr}(\omega \pm \Omega), \tag{30}$$

$$\begin{aligned} \sigma_r(\omega) = &-4 \frac{M^2}{\Omega} \int \frac{d\omega'}{2\pi}\, g_<(\omega') + M^2 P \int \frac{d\omega'}{2\pi} \left(\frac{g_>(\omega' - \Omega) + g_<(\omega' + \Omega)}{\omega - \omega'} \right) \\ &- i \frac{M^2}{2} (g_>(\omega - \Omega) + g_<(\omega + \Omega)). \end{aligned} \tag{31}$$

The greater-than (less-than) self-energies $\sigma_{>(<)}(\omega)$ describe the scattering out (in) of electrons at energy ω. The perturbation calculation presented here consists of the self-consistent solution of the resonant-site Green functions $g_r(\omega)$, $g_<(\omega)$ and the self-energies $\sigma_r(\omega)$, $\sigma_<(\omega)$ (using that the greater-than Green function is given by $g_>(\omega) = -2 \operatorname{Im} g_r(\omega) - g_<(\omega)$; see Eq.(15)). The expressions for these four functions are collected in Table II.

II.C. *The First Born Approximation*

In this subsection we calculate analytically the self-energies shown in Fig. 2 to first order in $g \equiv M^2/\Omega^2$, which corresponds to the first Born approximation. The escape rates $\Gamma_{L/R}$ are taken to be independent of energy. The analytical results for

the self-energies are used to discuss the qualitative behavior of the density of states, which with energy-independent escape rate $\Gamma = \Gamma_L + \Gamma_R$ becomes

$$2\pi N(\omega) = \frac{2(\Gamma - 2\,\mathrm{Im}\,\sigma_r(\omega))}{(\omega - E_r^0 - \mathrm{Re}\,\sigma_r(\omega))^2 + (\Gamma - \mathrm{Im}\,\sigma_r(\omega))^2}; \tag{32}$$

see Eqs. (20) and (22). In particular, the analytical expressions for the first-order self-energies allows the characterization of the two regimes **A** and **B**, both by the magnitude of the polaron shift, as well as by the (approximate) position of the satellite peaks. The study of the equilibrium polaron shift leads to the determination of the additional perturbation parameter, $g\Omega/\Gamma$, in Section II.E. The exact position of the satellite peak in the density of states is discussed further in Section II.F.

We consider resonant tunneling in the presence of an *optical* mode, and we shall consequently only discuss the case where the phonon frequency Ω is much greater than the total escape rate $\Gamma \equiv \Gamma_L + \Gamma_R$. Thus both here and throughout the paper we assume that $\Omega \gg \Gamma$. We evaluate the self-energies within the first Born approximation under the assumption of energy-independent escape rates, and the analytical expression obtained below is only correct if $\Gamma_L(\omega)$ and $\Gamma_R(\omega)$ do not vary with energy for $|\omega - E_r| < 2\Omega$.

The noninteracting Green functions $g_r^0(\omega)$ and $g_<^0(\omega)$ are given by Eqs. (20) and (21) with the self-energies set to zero: $\sigma_r(\omega) = \sigma_<(\omega) = 0$. With constant escape rate $\Gamma = \Gamma_L + \Gamma_R$, they can be written

$$g_r^0(\omega) = \frac{1}{\omega - E_r^0 + i\Gamma}, \tag{33}$$

$$g_<^0(\omega) = \frac{2\Gamma}{(\omega - E_r^0)^2 + \Gamma^2} f_{\mathrm{eff}}(\omega), \tag{34}$$

$$g_>^0(\omega) = \frac{2\Gamma}{(\omega - E_r^0)^2 + \Gamma^2} [1 - f_{\mathrm{eff}}(\omega)], \tag{35}$$

where we have introduced the effective distribution function $f_{\mathrm{eff}}(\omega)$ for the *noninteracting* problem

$$f_{\mathrm{eff}}(\omega) = g_<^0(\omega)/(-2\,\mathrm{Im}\,g_r^0(\omega)) = [\Gamma_L f_L(\omega) + \Gamma_R f_R(\omega)]/\Gamma. \tag{36}$$

To evaluate the first-order self-energies we substitute the noninteracting Green functions $g_<^0(\omega)$ and $g_r^0(\omega)$ for the self-consistent functions $g_<(\omega)$ and $g_r(\omega)$ in Eqs. (30) and (31). The integrals, which involve Lorentzians, are readily done at zero temperature, and the analytical expressions for the first-order self-energies, $\sigma^{(1)}(\omega)$, are listed in Table III.

Consider first the polaron shift $E_r - E_r^0 = \mathrm{Re}\,\sigma_r(\omega = E_r)$ (see Eq. (32)) of the resonant level. The first-order expression $\mathrm{Re}\,\sigma_r^{(1)}(\omega)$, listed in Table III, has logarithmic singularities at $\omega = \mu_L \pm \Omega$ and at $\omega = \mu_R \pm \Omega$ arising from the sharpness of the Fermi sea in the left and right leads. The contribution from these

TABLE III

The Self-Energies in the First Born Approximation (First Order in $g \equiv M^2/\Omega^2$), Evaluated for Constant Escape Rates $\Gamma_{L/R}$ and Zero Temperature, $1/\beta = 0$

$$\sigma_<^{(1)}(\omega) = M^2 \frac{2\Gamma}{(\omega+\Omega-E_r^0)^2+\Gamma^2} f_{\text{eff}}(\omega+\Omega), \qquad \sigma_>^{(1)}(\omega) = M^2 \frac{2\Gamma}{(\omega-\Omega-E_r^0)^2+\Gamma^2}[1-f_{\text{eff}}(\omega-\Omega)].$$

$$\text{Im}\,\sigma_r^{(1)}(\omega) = -\tfrac{1}{2}(\sigma_<^{(1)}(\omega)+\sigma_>^{(1)}(\omega)),$$

$$\begin{aligned}\text{Re}\,\sigma_r^{(1)}(\omega) = &-4\frac{M^2}{\Omega}P^0_{\text{occ}} + M^2P^0_{\text{occ}}\frac{(\omega+\Omega-E_r^0)}{(\omega+\Omega-E_r^0)^2+\Gamma^2} + M^2P^0_{\text{emp}}\frac{(\omega-\Omega-E_r^0)}{(\omega-\Omega-E_r^0)^2+\Gamma^2}\\ &- M^2\frac{1}{(\omega+\Omega-E_r^0)^2+\Gamma^2}\frac{\Gamma_L}{2\pi}\ln\left(\frac{(\omega+\Omega-\mu_L)^2}{(\mu_L-E_r^0)^2+\Gamma^2}\right) - M^2\frac{1}{(\omega+\Omega-E_r^0)^2+\Gamma^2}\frac{\Gamma_R}{2\pi}\ln\left(\frac{(\omega+\Omega-\mu_R)^2}{(\mu_R-E_r^0)^2+\Gamma^2}\right)\\ &+ M^2\frac{1}{(\omega-\Omega-E_r^0)^2+\Gamma^2}\frac{\Gamma_L}{2\pi}\ln\left(\frac{(\omega-\Omega-\mu_L)^2}{(\mu_L-E_r^0)^2+\Gamma^2}\right) + M^2\frac{1}{(\omega-\Omega-E_r^0)^2+\Gamma^2}\frac{\Gamma_R}{2\pi}\ln\left(\frac{(\omega-\Omega-\mu_R)^2}{(\mu_R-E_r^0)^2+\Gamma^2}\right).\end{aligned}$$

Using:

$$\Gamma_{L/R} \equiv \Gamma_{L/R}(E_r^0), \qquad \Gamma = \Gamma_L + \Gamma_R, \qquad f_{\text{eff}}(\omega) = \frac{\Gamma_L f_L(\omega) + \Gamma_R f_R(\omega)}{\Gamma},$$

$$P^0_{\text{occ}} \equiv \int \frac{d\omega}{2\pi} g^0_<(\omega) = \frac{\Gamma_L}{\Gamma}\left[\frac{1}{2}+\frac{1}{\pi}\arctan\left(\frac{\mu_L-E_r^0}{\Gamma}\right)\right] + \frac{\Gamma_R}{\Gamma}\left[\frac{1}{2}+\frac{1}{\pi}\arctan\left(\frac{\mu_R-E_r^0}{\Gamma}\right)\right],$$

$$P^0_{\text{emp}} \equiv \int \frac{d\omega}{2\pi} g^0_>(\omega) = \frac{\Gamma_L}{\Gamma}\left[\frac{1}{2}-\frac{1}{\pi}\arctan\left(\frac{\mu_L-E_r^0}{\Gamma}\right)\right] + \frac{\Gamma_R}{\Gamma}\left[\frac{1}{2}-\frac{1}{\pi}\arctan\left(\frac{\mu_R-E_r^0}{\Gamma}\right)\right].$$

Note. With the constant escape rate $\Gamma = \Gamma_L + \Gamma_R$ the noninteracting Green functions become $(g_r^0(\omega))^{-1} = \omega - E_r^0 + i\Gamma$ and $g_<^0(\omega) = -2\text{Im}\,g_r^0(\omega) f_{\text{eff}}(\omega)$, where $f_{\text{eff}}(\omega)$ is the effective distribution function for the noninteracting problem. Inserting $g_r^0(\omega)$ and $g_<^0(\omega)$ in the expressions for the self-energies (see Table II) produces the first-order estimates $\sigma_r^{(1)}(\omega)$ and $\sigma_{<,>}^{(1)}(\omega)$. P^0_{occ} and $P^0_{\text{emp}} = 1 - P^0_{\text{occ}}$ describe the filling condition of the resonant level. The polaron shift can be approximated by $\text{Re}\,\sigma_r^{(1)}(E_r^0)$ and typically only the first three terms of $\text{Re}\,\sigma_r^{(1)}(\omega)$ are important in determining the polaron shift. In regime **A** (**B**), where $P^0_{\text{emp}} = 1$ ($P^0_{\text{occ}} = 1$), a polaron shift of $-g\Omega$ ($-3g\Omega$) is found in the limit of $\Gamma \ll \Omega$. Note that without the Hartree diagram, which produces the first contribution to $\text{Re}\,\sigma_r^{(1)}(E_r^0)$, we would obtain the *incorrect* result of $+g\Omega$ for the polaron shift in regime **B**.

singular terms are, however, not important for $|\omega - \mu_{L/R} \pm \Omega| \gg \Gamma$. Hence, except at the special chemical potentials and biases, where $E_r \approx \mu_{L/R} \pm \Omega$, we can approximate the polaron shift by

$$\mathrm{Re}\,\sigma_r^{(1)}(E_r^0) \cong -4g\Omega P_{\mathrm{occ}}^0 + g\Omega \frac{\Omega^2}{\Omega^2+\Gamma^2} P_{\mathrm{occ}}^0 - g\Omega \frac{\Omega^2}{\Omega^2+\Gamma^2} P_{\mathrm{emp}}^0, \tag{37}$$

where the noninteracting probabilities for having an empty (occupied) resonant level are

$$P_{\mathrm{emp(occ)}}^0 \equiv \int \frac{d\omega}{2\pi}\, g_{>(<)}^0(\omega). \tag{38}$$

The polaron shift is therefore $\mathrm{Re}\,\sigma_r^{(1)}(E_r^0) \cong -g\Omega$ $(-3g\Omega)$ in regime **A** (**B**), where $P_{\mathrm{emp}}^0 = 1$ $(P_{\mathrm{occ}}^0 = 1)$, assuming that $\Gamma \ll \Omega$. These limits for the polaron shift are in agreement with the predictions of second-order perturbation theory (see Section I.C), but note that the contribution from the Hartree diagram, $-4g\Omega P_{\mathrm{occ}}^0$ in Eq. (37), is essential to obtain the correct behavior in regime **B**.

The noninteracting occupation probability for the resonant level, P_{occ}^0 listed in Table III, describes the filling condition of the resonant level. In equilibrium where $\mu_L = \mu_R = \mu$, the filling condition P_{occ}^0 is set by $(\mu - E_r)/\Gamma$, and the level is half occupied when $\mu = E_r$. Out of equilibrium the filling condition, P_{occ}^0, is set by Γ_L/Γ, and, as illustrated in Fig. 1, at a finite bias, where $\mu_L - E_r \gtrsim \Gamma$ and $E_r - \mu_R \gtrsim \Gamma$, regime **A** (**B**) is obtained if $\Gamma_L \ll \Gamma_R$ $(\Gamma_L \gg \Gamma_R)$. At such biases the level is half occupied if Γ_L is equal to Γ_R.

Within the first Born approximation it is possible to obtain analytically the functional form of the crossover between the two regimes **A** and **B** of different polaron shifts in equilibrium. Using again Table III with $\mu_L = \mu_R = \mu$, we find in the limit of $\Gamma \ll \Omega$ that

$$\mathrm{Re}\,\sigma_r^{(1)}(E_r^0) \approx -g\Omega - 2g\Omega\left[\frac{1}{2} + \arctan\left(\frac{\mu - E_r^0}{\Gamma}\right)\right]. \tag{39}$$

Note that the transition occurs on a scale of Γ about $\mu = E_r^0$. In particular at $\mu = E_r^0$ the slope is

$$\left.\frac{\partial(\mathrm{Re}\,\sigma_r^{(1)}(E_r^0))}{\partial\mu}\right|_{\mu=E_r^0} = -\frac{2}{\pi}\frac{g\Omega}{\Gamma}. \tag{40}$$

Next consider the position of the satellite peaks in the resonant-site spectral function or the density of states. Besides the main peak at $\omega = E_r$, the density of states will show satellite peaks arising from peaks in the inelastic scattering rate $-2\,\mathrm{Im}\,\sigma_r(\omega) = \sigma_<(\omega) + \sigma_>(\omega)$. The exact locations of these satellite peaks in the density of states are determined both by the inelastic scattering rate $-2\,\mathrm{Im}\,\sigma_r(\omega)$ and by the corresponding real part $\mathrm{Re}\,\sigma_r(\omega)$ of the self-energy (see Eq. (32)). This

is explained further in Section II.F. Here we use the analytical result for the first-order inelastic scattering rate, $-2\,\mathrm{Im}\,\sigma^{(1)}(\omega)$, to discuss the *approximate* position of the satellite peaks under different filling conditions of the resonant level.

Assuming constant escape rates, $\Gamma_{L/R}$, the first Born approximation for the scattering-in, $\sigma^{(1)}_{<}(\omega)$, and scattering-out, $\sigma^{(1)}_{>}(\omega)$, self-energies are

$$\sigma^{(1)}_{<}(\omega) = M^2 \frac{2\Gamma f_{\mathrm{eff}}(\omega+\Omega)}{(\omega+\Omega-E_r^0)^2+\Gamma^2}, \tag{41}$$

$$\sigma^{(1)}_{>}(\omega) = M^2 \frac{2\Gamma[1-f_{\mathrm{eff}}(\omega-\Omega)]}{(\omega-\Omega-E_r^0)^2+\Gamma^2}; \tag{42}$$

see Table III. In regime **A**, $f_{\mathrm{eff}}(\omega)$ is small for energies $|\omega - E_r| \lesssim \Gamma$, so $-2\,\mathrm{Im}\,\sigma_r^{(1)}(\omega)$ is given by the *scattering-out* self-energy $\sigma^{(1)}_{>}(\omega)$, which has a peak at $E_r^0+\Omega$. Similarly in regime **B**, $f_{\mathrm{eff}}(\omega)$ is large for $|\omega - E_r| \lesssim \Gamma$, and $-2\,\mathrm{Im}\,\sigma_r^{(1)}(\omega)$ is given by the *scattering-in* self-energy $\sigma^{(1)}_{<}(\omega)$, with a peak at $E_r^0-\Omega$. In the self-consistent Born approximation the inelastic scattering rate $-2\,\mathrm{Im}\,\sigma_r(\omega)$ will have a peak at $\omega = E_r+\Omega$ ($E_r-\Omega$) in regime **A** (**B**). The resonant-site spectral function or density of states will therefore show a satellite peak approximately at $E_r+\Omega$ ($E_r-\Omega$) in regime **A** (**B**) due to *scattering-out* (*scattering-in*) processes occurring when the resonant level is almost completely empty (occupied). When the resonant level is half occupied there will be two satellite peaks: one at approximately $E_r+\Omega$, corresponding to scattering-out processes, and one at approximately $E_r-\Omega$, corresponding to scattering-in processes.

II.D. *The Equilibrium Resonant-Site Density of State*

Figure 3 shows the dependence of the equilibrium resonant-site density of states $N(\omega) = -\mathrm{Im}\,g_r(\omega)/\pi$ on the filling condition. We set $E_r^0 = 0$ as indicated by the dotted line; the parameters are listed in Table I. As expected the interacting density of states in regime **A** (upper panel) shows a small negative polaron shift $E_r = -g\Omega$ and has a satellite peak above the resonant level at $\omega \approx E_r+\Omega$, arising from scattering-out processes with final energy E_r. Note that the position of the satellite peak is located slightly above $E_r+\Omega$, as explained in Section II.F below. In regime **B**, the interacting density of states (solid curve on lower panel) has larger negative polaron shift $E_r = -3g\Omega$ and a satellite peak at $\omega \approx E_r-\Omega$, arising from scattering-in processes with initial energy E_r. The position of the satellite peak is now located slightly below $E_r-\Omega$, as also explained in Section II.F. Note that already at $\mu = E_r^0 = 0$ we are in regime **B**. Also shown in the lower panel for reference is the noninteracting, resonant-site density of states $N^0(\omega) = -\mathrm{Im}\,g_r^0(\omega)/\pi$ (dashed-dotted curve). The middle panel shows the interacting density of states $N(\omega)$ when $\mu = E_r$ and the resonant level is half occupied. Here the interacting density of states has an intermediate negative polaron shift $E_r = -2g\Omega$ and *two* satellite peaks at $\omega \approx E_r \pm \Omega$. The satellite peak at $\omega \approx E_r + (-)\Omega$ for the *equilibrium* density of states has a distorted shape since only half of the resonant level at $E_r = \mu$ is available for scattering-out (scattering-in) processes: no scattering-out (scattering-in) can occur

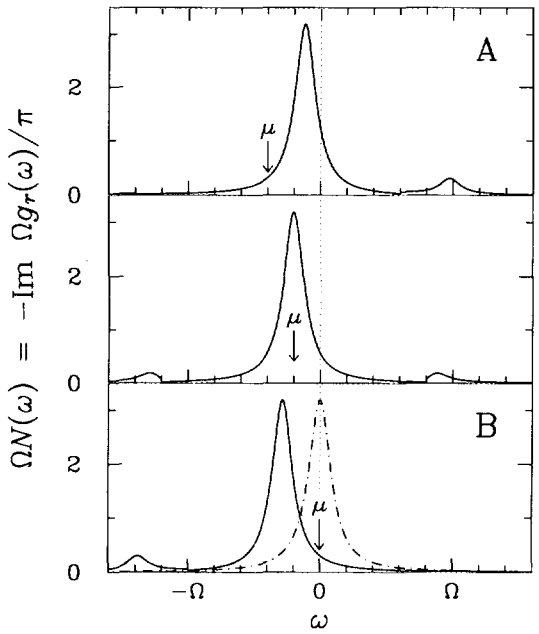

FIG. 3. Dependence of the *equilibrium* resonant-site density of states $N(\omega) = -\text{Im}\, g_r(\omega)/\pi$ on the filling condition (set by $\mu - E_r$). In the upper (lower) panel regime **A** (**B**) is obtained since the resonant level is nearly empty (occupied). The density of states in regime **A** (shown in the upper panel) has a small negative polaron shift $E_r = -g\Omega$ ($g = 0.1$; $E_r^0 = 0$) and a satellite peak slightly above $\omega = E_r + \Omega$ (see also Fig. 5 and Section II.F) arising from *scattering-out* processes with final energy E_r. The density of states in regime **B** (solid curve in lower panel) has a larger negative polaron shift $E_r = -3g\Omega$ and a satellite peak slightly below $\omega = E_r - \Omega$ (see Section II.F) arising from *scattering-in* processes with initial energy E_r. Note that regime **B** is obtained already when $\mu = E_r^0 = 0$ (see also Fig. 4). The noninteracting density of states $N^0(\omega) = -\text{Im}\, g_r^0(\omega)/\pi$ (dash-dotted curve in the lower panel) is shown for reference. When $\mu = E_r$, the resonant site is half occupied and the interacting density of states $N(\omega)$ (shown in the middle panel) has an intermediate negative shift $E_r = -2g\Omega$ and *two* satellite peaks. The distorted shape of the satellite peak at $\omega \approx E_r + (-)\Omega$ is due to only half the resonant level being available for the scattering-out (scattering-in) processes: no scattering-out (scattering-in) can occur at energies $\omega < \mu + \Omega$ ($\omega > \mu - \Omega$) because the final (initial) states are occupied (empty). The scattering-out (scattering-in) satellite peak above (below) the resonance rises (drops) dramatically exactly at $\omega = \mu + \Omega$ ($\omega = \mu - \Omega$) because of the large density of final (initial) states for scattering-out (scattering-in) processes at $\mu = E_r$. The parameters used in this equilibrium study are listed in Table I.

at energies $\omega < \mu + \Omega$ ($\omega > \mu - \Omega$) because the final (initial) states are occupied (empty). The scattering-in (scattering-out) satellite peak above (below) E_r rises (drops) dramatically exactly at $\omega = \mu + \Omega$ ($\omega = \mu - \Omega$) because of the large density of final (initial) states at $\mu = E_r$ [53].

II.E. *The Equilibrium Polaron Shift and the Perturbation Parameter*

The set of crosses in the upper panel of Fig. 4 shows the equilibrium polaron shift $E_r(\mu) (\equiv E_r(\mu) - E_r^0$; parameters are the same as in Fig. 3) calculated in the

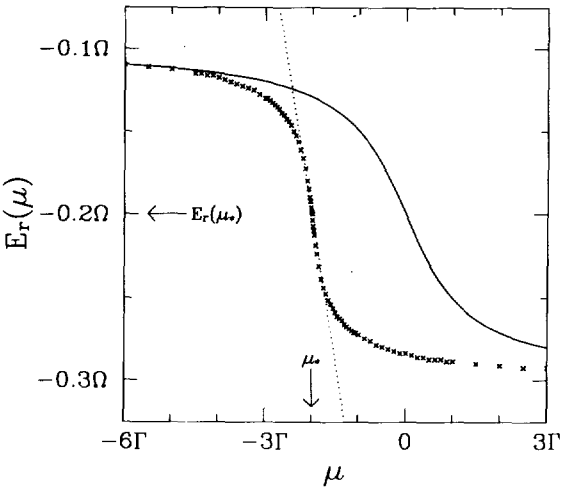

FIG. 4. The equilibrium polaron shift $E_r(\mu)$ ($\equiv E_r(\mu) - E_r^0$; parameters are the same as in Fig. 3) *versus* the filling condition set by chemical potential μ. The energy scale of the abscissa is $\Gamma \equiv \Gamma_L + \Gamma_R$, where $\Gamma_{L/R} \equiv \Gamma_{L/R}(E_r^0 = 0)$. In the self-consistent calculation (crosses) the polaron shift $E_r(\mu)$ changes from approximately $-g\Omega = -0.1\Omega$ for $\mu - E_r \ll -\Gamma$, to approximately $-3g\Omega = -0.3\Omega$ for $\mu - E_r \gg \Gamma$, consistent with second-order perturbation theory. The solid curve shows the first-order estimate $\mathrm{Re}\,\sigma_r^{(1)}$ ($E_r^0 = 0$) for the polaron shift, evaluated for constant escape rates $\Gamma_{L/R}$. The crossover between the two regimes of different polaron shifts occurs in the first-order estimate at $\mu = 0$ with slope $-(2g\Omega)/(\pi\Gamma)$. In the self-consistent Born approximation (crosses) the crossover occurs at $\mu_* = E_r(\mu_*)$, with slope $(\partial E_r/\partial\mu)_{\mu=\mu_*} \approx -(2/\pi)(g\Omega/\Gamma)/[1-(2/\pi)(g\Omega/\Gamma)]$, as indicated by the dotted line. Note that this slope of the polaron shift becomes singular at $\mu = \mu_*$ when $(2g\Omega)/(\pi\Gamma) \to 1$, and the self-consistent Born approximation is limited to small values of $g\Omega/\Gamma$. Thus, while the Born approximation treats the interaction to lowest order in g, there is an additional perturbation parameter $g\Omega/\Gamma$.

self-consistent Born approximation *versus* chemical potential μ. As expected the polaron shift interpolates between a small shift of $-g\Omega$ for $\mu - E_r \ll -\Gamma$ to a larger negative shift of $-3g\Omega$ for $\mu - E_r \gg \Gamma$. The solid curve on the upper panel of Fig. 4 shows the first-order estimate Eq. (39) for the polaron shift $E_r^{(1)}(\mu)$ ($\equiv E_r^{(1)}(\mu) - E_r^0$), which also interpolates between these limits, but more gradually. This is surprising because for $g \ll 1$ one expects the first-order result to be a good approximation to the self-consistent calculation.

To understand this discrepancy let us try to estimate the self-consistent polaron shift near the point where the equilibrium chemical potential is at the resonant level, $\mu_* = E_r(\mu_*)$. The position of the resonant level $E_r(\mu)$ is determined by

$$E_r(\mu) - E_r^0 - \mathrm{Re}\,\sigma_r(\mu, \omega = E_r(\mu)) = 0. \tag{43}$$

To approximate the value of $\mathrm{Re}\,\sigma_r(\mu, E_r(\mu))$ in the self-consistent calculation, we substitute $E_r(\mu)$ for E_r^0 in the expression for $\mathrm{Re}\,\sigma_r^{(1)}$ ($\omega = E_r(\mu)$); see

Table III. We neglect the logarithmic terms in estimating the resonant level $E_r(\mu)$ by

$$E_r(\mu) - E_r^0 + 2g\Omega + \frac{2g\Omega}{\pi}\left[2 - \frac{1}{1+(\Gamma/\Omega)^2}\right] \arctan\left(\frac{\mu - E_r(\mu)}{\Gamma}\right) = 0. \tag{44}$$

The slope of the polaron shift at $\mu_* = E_r(\mu_*)$ is obtained by differentiating with respect to μ. To lowest order in Γ/Ω we obtain

$$\left.\frac{\partial E_r(\mu)}{\partial \mu}\right|_{\mu=\mu_*} \approx \frac{-(2g\Omega)/(\pi\Gamma)}{1-(2g\Omega)/(\pi\Gamma)}. \tag{45}$$

The estimate Eq. (45) for the slope of the polaron shift at μ_* is indicated by the dotted curve on Fig. 4 and agrees well with the result of self-consistent calculation. Thus, the discrepancy between the first-order calculation and the self-consistent calculation results because the dimensionless parameter, $g\Omega/\Gamma$, is large ($g\Omega/\Gamma \approx 1$). When $(2g\Omega)/(\pi\Gamma) \to 1$, the estimate Eq. (45) for the slope of the polaron shift at μ_* becomes singular.

The quantity $g\Omega/\Gamma$ is a new perturbation parameter in the study of the equilibrium, zero-temperature polaron shift, in addition to the obvious parameter g. The parameter $g\Omega/\Gamma$ is the ratio of the *difference* in polaron shifts in the two regimes **A** and **B** to the width Γ of the resonance peak of the density of states $N(\omega)$. When the ratio $g\Omega/\Gamma$ becomes comparable to 1, the spectral weight of $N(\omega)$ can be polaron shifted from being mostly above the chemical potential μ to being mostly below μ when the chemical potential is increased past $\mu_* = E_r(\mu_*)$. Hence the difference in polaron shift between regime **A** and **B** causes the system to change rapidly between the two regimes, and for large values of $g\Omega/\Gamma$ the equilibrium polaron shift becomes singular at $\mu_* = E_r(\mu_*)$.

We also note that the same perturbation parameter, $g\Omega/\Gamma$, enters in the evaluation of the resonant-site density of states $N(\omega) = -\text{Im}\, g_r(\omega)/\pi$; to lowest order in g the density of states actually becomes negative at $\omega = E_r^0 + \Gamma$ if $g\Omega/\Gamma > \frac{1}{2}$. This additional perturbation parameter is important in the physically relevant case of $\Omega \gg \Gamma$ that we consider here.

We have chosen to show calculations for $g\Omega/\Gamma \approx 1$. We find qualitatively the same behavior in the reported self-consistent calculations as found in calculations for smaller, and more appropriate, values of $g\Omega/\Gamma$. However, the effects of the interaction are more clearly visible for the larger value $g\Omega/\Gamma \approx 1$ that we have used.

II.F. *The Position of the Satellite Peak*

The position of the satellite peak in the resonant-site spectral function or density of states $N(\omega) = -\text{Im}\, \sigma_r(\omega)/\pi$ calculated within the self-consistent Born approximation (shown in Fig. 3) is shifted in regime **A** (**B**) up (down) from the peak position $E_r + \Omega$ ($E_r - \Omega$) of the inelastic scattering rate, $\text{Im}\, \sigma_r(\omega)$. Note that $\Omega = 10\Gamma$, and the upward (downward) shift in regime **A** (**B**) is approximately Γ.

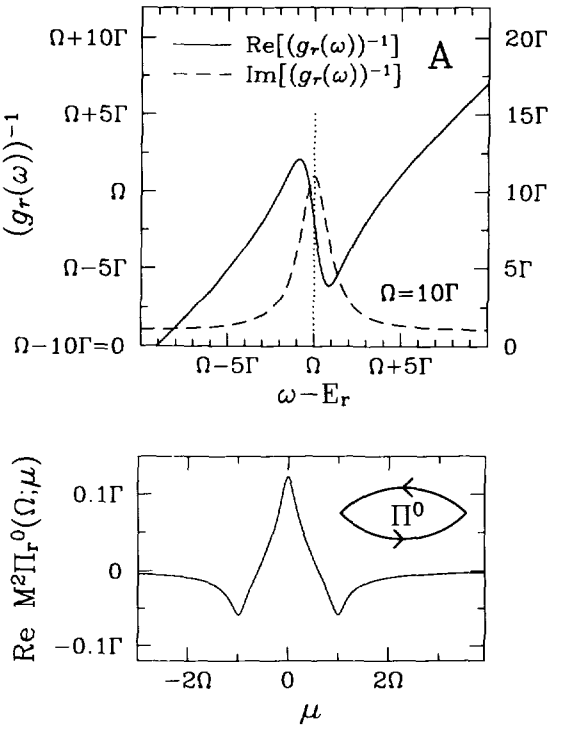

FIG. 5. Energy dependence of $\mathrm{Re}[g_r(\omega)^{-1}]$ and $\mathrm{Im}[g_r(\omega)^{-1}]$ (upper panel) in equilibrium regime A explaining the position of the satellite peak in the density of states $N(\omega) = -\mathrm{Im}\, g_r(\omega)/\pi$ (see Fig. 3); *and* the lowest order renormalization, $M^2\,\mathrm{Re}\,\Pi_r^0(\Omega;\mu)$, of the phonon frequency (lower panel) versus the chemical potential μ ($\equiv \mu - E_r^0$; parameters are the same as in Fig. 3). The energy scale of the ordinate is $\Gamma = \Gamma_L + \Gamma_R$, where $\Gamma_{L/R} = \Gamma_{L/R}(E_r^0 = 0)$. The free phonon frequency is $\Omega = 10\Gamma$. The *upper* panel shows the energy dependence of $\mathrm{Re}[g_r(\omega)^{-1}] \approx \omega - E_r^0 - \mathrm{Re}\,\sigma_r(\omega)$ (solid curve) and $\mathrm{Im}[g_r(\omega)^{-1}] \approx \Gamma - \mathrm{Im}\,\sigma_r(\omega)$ (dashed curve) at chemical potential μ corresponding to upper panel of Fig. 3. The self-energies $\mathrm{Re}\,\sigma_r(\omega)$ and $\mathrm{Im}\,\sigma_r(\omega)$ are evaluated assuming constant escape rates $\Gamma_{L/R}$ within the first Born approximation (see Table III), however, with the interacting resonant level E_r substituted for E_r^0 (and neglecting the logarithmic contributions). In regime A the satellite peak in the density of states is shifted up from the peak position, $\omega = E_r + \Omega$ (indicated by dotted line), of the inelastic scattering rate ($-2\,\mathrm{Im}\,\sigma_r(\omega)$) towards $\omega = E_r + \Omega + \Gamma$ because of the dramatic energy dependence of $\omega - E_r^0 - \mathrm{Re}\,\sigma_r(\omega)$ at $\omega \approx E_r + \Omega$. In regime **B** (not shown) the energy dependence of $\omega - E_r^0 - \mathrm{Re}\,\sigma_r(\omega)$ at $\omega \approx E_r - \Omega$ similarly shifts the satellite peak from $\omega = E_r - \Omega$ down towards $\omega = E_r - \Omega - \Gamma$. The *lower* panel shows the renormalization, $M^2\,\mathrm{Re}\,\Pi_r^0$ ($\omega = \Omega; \mu$), of the phonon frequency in equilibrium as a function of chemical potential μ. This renormalization is determined by calculating the lowest order retarded polarization insertion $\Pi_r^0(\omega;\mu)$ (with the diagram shown in the insert), assuming constant escape rates $\Gamma_{L/R}$ (see Table IV). Note that the phonon renormalization is at most about 1% of the free phonon frequency $\Omega = 10\Gamma$. Also note that the phonon renormalization is at (at least) an order of magnitude smaller than the upwards or downwards shifts (of the satellite peak position) which result from the Born approximation self-energy effect illustrated for regime A in the upper panel.

To understand this shift it is necessary to consider both the real and imaginary parts of the retarded self-energy, $\sigma_r(\omega)$. The upper panel of Fig. 5 shows the approximations $\mathrm{Re}(g_r(\omega))^{-1} \approx \omega - E_r^0 - \mathrm{Re}\,\sigma_r(\omega)$ (solid curve) and $\mathrm{Im}(g_r(\omega))^{-1} \approx \Gamma - \mathrm{Im}\,\sigma_r(\omega)$ (dashed curve), for the case corresponding to the upper panel of Fig. 3. The constant escape rate $\Gamma = \Gamma_L + \Gamma_R$ (with $\Gamma_{L/R} = \Gamma_{L/R}(E_r^0)$) have been assumed, and the self-energies are evaluated using the first Born approximations (see Table III), with E_r substituted for E_r^0 (and neglecting the logarithmic contributions). The nominator, $2(\Gamma - \mathrm{Im}\,\sigma_r(\omega))$, of the approximation equation (32) for the density of state, is of course (like the regime **A** inelastic scattering rate) peaked at $\omega = E_r + \Omega$. However, the dramatic energy dependence of $\mathrm{Re}(g_r(\omega))^{-1} \approx \omega - E_r^0 - \mathrm{Re}\,\sigma_r(\omega)$ (entering in the denominator) shifts the position of the regime **A** satellite peak up towards $\omega = E_r + \Omega + \Gamma$. In regime **B** (not shown) the energy dependence of $\omega - E_r - \mathrm{Re}\,\sigma_r(\omega)$ at $\omega \approx E_r - \Omega$ similarly shifts the position of the satellite peak down from $\omega = E_r - \Omega$ (peak position of the regime **B** inelastic scattering rate) towards $\omega = E_r - \Omega - \Gamma$.

In both regimes we therefore find that the separation between the main peak and the satellite peak of the density of state is approximately $\Omega + \Gamma$, where $\Omega = 10\Gamma$ is the free phonon frequency. However, to determine the exact position of the satellite peak we must also consider the possible renormalization of the phonon frequency. The self-consistent Born approximation used in this paper assumes that the phonon mode retains the free phonon frequency Ω, and remains in equilibrium. The electron–phonon interaction will, however, renormalize the phonon frequency to an interacting value Ω'. If this renormalization is significant it would result in a different separation between the main and satellite peaks of the density of state than the value, $\Omega + \Gamma$, obtained within the Born approximation. Below we verify that the lowest order renormalization of the phonon frequency can in fact be neglected and that this renormalization does not significantly modify the above discussion of the satellite peak position.

To calculate the renormalization of the phonon frequency we consider the retarded polarization insertion [54]

$$\Pi_r(t-t') = -i\Theta(t-t')\langle[c_0^+(t)\,c_0(t),\, c_0^+(t')\,c_0(t')]\rangle. \tag{46}$$

In the noninteracting case this correlation function can be represented by the diagram shown in the insert of Fig. 5 (lower panel). Upon Fourier transforming in $t-t'$ the result for the noninteracting retarded polarization insertion $\Pi_r^0(\omega)$ becomes

$$\Pi_r^0(\omega) = \int \frac{d\omega'}{2\pi}\,[g_r^0(\omega'+\omega)\,g_<^0(\omega') + g_<^0(\omega'+\omega)\,g_a^0(\omega')]. \tag{47}$$

If constant escape rates $\Gamma_{L/R}$ can be assumed, this integral, involving Lorentzians, can easily be done at zero temperature and the analytical expressions for the real and imaginary parts of $\Pi_r^0(\omega)$ are listed in Table IV.

TABLE IV

The Lowest-Order Polarization Insertion $\Pi_r^0(\omega)$ Evaluated Assuming Constant Escape Rates $\Gamma_{L/R}$ and Zero Temperature, $1/\beta = 0$

$$
\begin{aligned}
2\pi(\omega^2+4\Gamma^2)\,\mathrm{Re}\,\Pi_r^0(\omega) = {} & \Gamma_L\left[\ln\left(\frac{(\mu_L-E_r^0+\omega)^2+\Gamma^2}{(\mu_L-E_r^0)^2+\Gamma^2}\right)+\ln\left(\frac{(\mu_L-E_r^0-\omega)^2+\Gamma^2}{(\mu_L-E_r^0)^2+\Gamma^2}\right)\right] \\
& +\Gamma_R\left[\ln\left(\frac{(\mu_R-E_r^0+\omega)^2+\Gamma^2}{(\mu_R-E_r^0)^2+\Gamma^2}\right)+\ln\left(\frac{(\mu_R-E_r^0-\omega)^2+\Gamma^2}{(\mu_R-E_r^0)^2+\Gamma^2}\right)\right] \\
& -\frac{4\Gamma}{\omega}\Gamma_L\left[\arctan\left(\frac{\mu_L-E_r^0+\omega}{\Gamma}\right)-\arctan\left(\frac{\mu_L-E_r^0-\omega}{\Gamma}\right)\right] \\
& -\frac{4\Gamma}{\omega}\Gamma_R\left[\arctan\left(\frac{\mu_R-E_r^0+\omega}{\Gamma}\right)-\arctan\left(\frac{\mu_R-E_r^0-\omega}{\Gamma}\right)\right], \\
-2\pi(\omega^2+4\Gamma^2)\,\mathrm{Im}\,\Pi_r^0(\omega) = {} & 2\Gamma_L\left[\arctan\left(\frac{\mu_L-E_r^0+\omega}{\Gamma}\right)-\arctan\left(\frac{\mu_L-E_r^0-\omega}{\Gamma}\right)\right] \\
& +2\Gamma_R\left[\arctan\left(\frac{\mu_R-E_r^0+\omega}{\Gamma}\right)-\arctan\left(\frac{\mu_R-E_r^0-\omega}{\Gamma}\right)\right] \\
& +\frac{2\Gamma}{\omega}\Gamma_L\left[\ln\left(\frac{(\mu_L-E_r^0+\omega)^2+\Gamma^2}{(\mu_L-E_r^0)^2+\Gamma^2}\right)+\ln\left(\frac{(\mu_L-E_r^0-\omega)^2+\Gamma^2}{(\mu_L-E_r^0)^2+\Gamma^2}\right)\right] \\
& +\frac{2\Gamma}{\omega}\Gamma_R\left[\ln\left(\frac{(\mu_R-E_r^0+\omega)^2+\Gamma^2}{(\mu_R-E_r^0)^2+\Gamma^2}\right)+\ln\left(\frac{(\mu_R-E_r^0-\omega)^2+\Gamma^2}{(\mu_R-E_r^0)^2+\Gamma^2}\right)\right].
\end{aligned}
$$

Using:

$$\Gamma_{L/R} \equiv \Gamma_{L/R}(E_r^0), \qquad \Gamma = \Gamma_L + \Gamma_R.$$

Note. The value of $M^2\,\mathrm{Re}\,\Pi_r^0\,(\omega=\Omega)$ determines the renormalization of the phonon frequency from the free value, Ω. For the equilibrium high-doping situation the renormalization, $M^2\,\mathrm{Re}\,\Pi_r^0\,(\omega=\Omega;\mu)$ (shown for $\Gamma=\Gamma_L+\Gamma_R$ with $\Gamma_{L/R}=\Gamma_{L/R}(E_r^0)$ and $g=0.1$ on lower panel of Fig. 5 as a function of chemical potential μ) is at most about 1% of the free phonon frequency. The renormalization of the phonon frequency can in general be neglected for $g=0.1$ when $\Omega \gg \Gamma$.

The renormalization, $\Omega'-\Omega$, of the phonon frequency is to lowest order in $g=M^2/\Omega^2$ given by

$$\Omega'-\Omega \approx M^2\,\mathrm{Re}\,\Pi_r^0\,(\omega=\Omega). \tag{48}$$

The lower panel of Fig. 5 shows this renormalization in equilibrium (using $\Gamma=\Gamma_L+\Gamma_R$ with $\Gamma_{L/R}=\Gamma_{L/R}(E_R^0)$; parameters same as in Fig. 3) as a function of the chemical potential μ. Note that the renormalization is at most about 1% of the free phonon frequency $\Omega=10\Gamma$. The renormalization is in general (also with a finite applied bias) insignificant for $g=0.1$ when $\Omega \gg \Gamma$. In particular, the renormalization of the phonon frequency is (at least) an order of magnitude smaller than the shift of the satellite peak position resulting from the Born-approximation self-energy effect illustrated for regime A in the upper panel of Fig. 5.

III. The Nonlinear Current

In this section, we study the nonlinear transport using the nonequilibrium Green functions evaluated within the self-consistent Born approximation. We demonstrate that current is conserved and calculate the nonlinear current–voltage characteristic. We furthermore study the current density per unit energy at the resonant site and in the left and right leads. Finally, we separate the current densities for the leads into elastic and inelastic contributions, which we study in a typical example.

III.A. *General Expressions for the Current*

The number-currents running from the left lead to the resonance level, I_L, and from the resonance level to the right lead, I_R, are

$$I_L = 2iW_L[\langle c_0^+ c_{-1}\rangle - \langle c_{-1}^+ c_0\rangle], \tag{49}$$

$$I_R = 2iW_R[\langle c_1^+ c_0\rangle - \langle c_0^+ c_1\rangle]. \tag{50}$$

There is a factor of 2 for spin. These currents can be expressed in terms of the resonant-site Green functions as [25, 28, 30, 32]

$$I_{L/R} = 2\int_{-\infty}^{\infty} \frac{d\omega}{2\pi} I_{L/R}(\omega), \tag{51}$$

$$I_L(\omega) = 2\Gamma_L(\omega)[2\pi N(\omega) f_L(\omega) - g_<(\omega)], \tag{52}$$

$$I_R(\omega) = 2\Gamma_R(\omega)[g_<(\omega) - 2\pi N(\omega) f_R(\omega)]. \tag{53}$$

$I_L(\omega)$ ($I_R(\omega)$) is the current density per unit energy and per spin, which flows through the left (right) barrier into (out from) the resonant level. It is straightforward to show, using the general expressions for the Green function listed in Ref. [30], that $I_L(\omega)$ ($I_R(\omega)$) is also the current density anywhere in the left (right) lead. In the steady state situation considered here, the continuity equation becomes

$$0 \equiv I_L - I_R = 2\int_{-\infty}^{\infty} \frac{d\omega}{2\pi} [\sigma_>(\omega)\, g_<(\omega) - \sigma_<(\omega)\, g_>(\omega)]. \tag{54}$$

The factor $\sigma_>(\omega)\, g_<(\omega)$($\sigma_<(\omega)\, g_>(\omega)$) can be interpreted as the scattering-out (scattering-in) rate, and the integrand of Eq. (54) is thus the *net* scattering-out rate. The self-consistent Born approximation satisfies the continuity equation, i.e., conserves current, because

$$\sigma_>(\omega)\, g_<(\omega) = M^2 g_>(\omega - \Omega)\, g_<(\omega), \tag{55}$$

$$\sigma_<(\omega)\, g_>(\omega) = M^2 g_<(\omega + \Omega)\, g_>(\omega), \tag{56}$$

and the two contributions in Eq. (54) cancel upon integration.

The noninteracting current I_0 is given by the Tsu–Esaki formula [15], an example of a Landauer–Büttiker formula [1, 2]. Because there are no interactions,

the tunneling of each electron is independent and the tunneling probability for a single electron is given by a noninteracting transmission coefficient $T_0(\omega)$, obtained by simple wave mechanics. It is related to the noninteracting resonant-site density of states $N^0(\omega) = -\text{Im}\, g_r^0(\omega)/\pi$ by

$$T_0(\omega) = \frac{2\Gamma_L(\omega)\,\Gamma_R(\omega)}{\Gamma_L(\omega)+\Gamma_R(\omega)}\, 2\pi N^0(\omega). \tag{57}$$

In the Tsu–Esaki formula the noninteracting current is then calculated by simply summing up the contribution $T_0(\omega)$ from energy ω

$$I_0 = 2\int_{\mu_R}^{\mu_L} \frac{d\omega}{2\pi} \frac{2\Gamma_L(\omega)\,\Gamma_R(\omega)}{\Gamma_L(\omega)+\Gamma_R(\omega)}\, 2\pi N^0(\omega)[f_L(\omega) - f_R(\omega)]. \tag{58}$$

Note that the integration is restricted to the range from μ_R to μ_L, as indicated in Eq. (58), because we discuss a system at zero temperature.

A natural question to ask is whether the interacting current $I = I_L = I_R$ can be written in a form similar to Eq. (58). As shown by Hershfield *et al.* [25], Meir and Wingreen [28], and in an earlier paper [32], the interacting current can be written as a sum of two terms,

$$I = I_a + I_c, \tag{59}$$

where the leading term, I_a, is indeed formally similar to Eq. (58). We refer to I_a as the density-of-states term, and to the other term, I_c, as the correction term

$$I_a = 2\int_{\mu_R}^{\mu_L} \frac{d\omega}{2\pi} \frac{2\Gamma_L(\omega)\,\Gamma_R(\omega)}{\Gamma_L(\omega)+\Gamma_R(\omega)}\, 2\pi N(\omega)[f_L(\omega) - f_R(\omega)], \tag{60}$$

$$I_c = 2\int_{-\infty}^{\infty} \frac{d\omega}{2\pi} \frac{1}{2} \frac{\Gamma_L(\omega)-\Gamma_R(\omega)}{\Gamma_L(\omega)+\Gamma_R(\omega)} [\sigma_>(\omega)\, g_<(\omega) - \sigma_<(\omega)\, g_>(\omega)]. \tag{61}$$

Often it is possible to neglect the energy-dependence of $\Gamma_L(\omega)$ and $\Gamma_R(\omega)$ for all relevant energies, $|\omega - E_r| < 2\Omega$. The integrand in Eq. (61),

$$I_c(\omega) \equiv \frac{1}{2} \frac{\Gamma_L(\omega)-\Gamma_R(\omega)}{\Gamma_L(\omega)+\Gamma_R(\omega)} [\sigma_>(\omega)\, g_<(\omega) - \sigma_<(\omega)\, g_>(\omega)], \tag{62}$$

is then given by the net scattering out rate $\sigma_>(\omega)\, g_<(\omega) - \sigma_<(\omega)\, g_>(\omega)$, and the correction term I_c is zero, because of current conservation, Eq. (54). Also with constant escape rates we have

$$I \approx I_a \propto \int_{\mu_R}^{\mu_L} N(\omega)\, d\omega. \tag{63}$$

Thus in this case the shape of the resonant-site density of states $N(\omega) = -\text{Im}\, g_r(\omega)/\pi$ determines the current. Note finally that if the escape rates are energy independent and if we are in a high-bias limit with $\mu_L - E_r \gg \Omega$ and $E_r - \mu_R \gg \Omega$, the current becomes insensitive to the interaction, because the total spectral weight of $N(\omega) = -\text{Im}\, g_r(\omega)/\pi$ is 1, irrespective of the strength and type of interaction [32].

III.B. *The Nonlinear Current–Voltage Characteristic*

In this subsection we study the current–voltage (I-V) characteristic in two examples, which we call the high-doping and the low-doping cases. In the high-doping case, where the Fermi seas of the two leads are thick, the current is insensitive to the interaction at typical biases. In contrast, for the low-doping case, where the

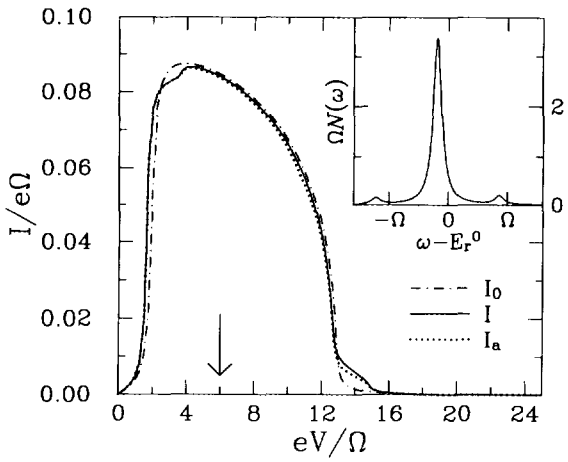

FIG. 6. The I-V characteristic in the high-doping case, where the depth of the Fermi sea, $\mu + 2W$, is large compared to Ω. The escape rates are equal in equilibrium; the parameters are listed in Table I. The density-of-states term I_a (dotted curve) (see Eq. (60)) is in general an excellent approximation to the interacting current (solid curve). The correction $I_c = I - I_a$ (see Eq. (61)) is only significant when a shoulder in the current is observed for $13\Omega < eV < 15\Omega$. The interacting current I (solid curve) and the noninteracting current I_0 (dash-dotted curve) are also very similar. They both show an onset of a large resonant current at bias $eV = 2\Omega$, which persist until the valley region at bias $eV > 13\Omega$, where the lower band-edge of the left lead, ϕ_L, is pushed above E_r. Major differences are: (1) The small suppression of the interacting current I at biases $eV \approx 2\Omega$ to $eV \approx 4\Omega$, which arises because the full weight of the interacting, resonant-site density of states $N(\omega) = -\text{Im}\, g_r(\omega)/\pi$ is not yet included in the integral Eq. (63) proportional to $I_a \approx I$. At biases from $eV = 2\Omega$ to $eV = 12\Omega$, the escape rates are approximately equal, and the resonant level is half occupied. As illustrated in the insert for bias $eV = 6\Omega$ (indicated by the arrow) the density of states therefore has two satellite peaks, and for biases in the range of $2\Omega < eV < 4\Omega$ the upper satellite peak is not included, leading to a small reduction of I. (2) A shoulder in the interacting current at biases from $eV = 13\Omega$ to $eV \approx 15\Omega$, which results from electrons tunneling inelastically via the emission of a phonon. The shoulder is observed in the valley region, where $\phi_L > E_r$, and there is only a very small noninteracting current. In the presence of interactions, however, electrons can enter at energy $E_r + \Omega$, emit a phonon, and thus tunnel inelastically. Note that the shoulder persist until at bias $eV = 15\Omega$, ϕ_L is pushed above $E_r + \Omega$.

thickness of the Fermi sea is comparable to the phonon frequency, the interacting and noninteracting currents differ significantly. We have also reduced the bandwidth in the low-doping case to cause the escape rates to be more energy dependent and to make the correction term I_c more important in the valley region. In both cases we have $\Omega \gg \Gamma_L(\omega) + \Gamma_R(\omega)$.

High-Doping Case. Figure 6 shows the nonlinear current–voltage (I-V) characteristic in the high-doping case. The thickness of the equilibrium Fermi sea is $\mu + 2W = 5.5\Omega$, the bandwidth is $4W = 20\Omega$ and the escape rates are equal in equilibrium; the parameters are listed in Table I. The I-V characteristic shows an onset of a large resonant current when the resonant level enters the Fermi sea of the left lead at $eV \approx 2\Omega$. The large resonant current slowly decreases until at $eV \approx 13\Omega$ the system enters the valley region, where the lower band-edge ϕ_L is pushed above resonant level E_r. The slow decrease of the resonant current as the bias approaches the valley region is a consequence of $\Gamma_L(E_r)/\Gamma_R(E_r)$, decreasing when $\phi_L \to E_r$.

As expected from Section III.A, when the energy dependence of the escape rates is weak, the density-of-states term I_a (dotted curve) is an excellent approximation to the interacting current I (solid curve). The correction $I_c = I - I_a$ is significant only when a shoulder in the current is observed ($13\Omega < eV < 15\Omega$). Also, the interacting current I (solid curve) and the noninteracting current I_0 (dash-dotted curve) are approximately equal, but not as close as I and I_a. The onset of the large resonant current occurs at a lower applied bias for I than for I_0, because of the polaron shift with the interaction, but at peak value they agree to within a few percent. However, there are two places where the interacting current I differs significantly from the noninteracting current I_0: (1) a small suppression of I ($2\Omega < eV < 4\Omega$) right after the onset of the resonant current and (2) a shoulder in the interacting current in the valley region. These differences are discussed below.

(1) The small suppression of the current at biases between 2Ω and 4Ω arises because the limit of integration from μ_R to μ_L in Eq. (60) does not yet include the upper satellite peak of the nonequilibrium density of states $N(\omega)$. At biases where there is a large resonant current, $2\Omega < eV < 12\Omega$, the escape rates are approximately equal for $|\omega - E_r| \lesssim (\Gamma_L(E_r) + \Gamma_R(E_r))$, and the resonant level is half occupied. Thus the density of states $N(\omega) = -\mathrm{Im}\, g_r(\omega)/\pi$ has two satellite peaks, as illustrated in the insert, which shows $N(\omega)$ at bias $eV \approx 6\Omega$ (bias indicated by arrow). At biases from 2Ω to 4Ω the spectral weight of $N(\omega)$ in the upper satellite peak is not yet included in the integral Eq. (60) for I_a. The noninteracting current I_0 is given by a similar integral Eq. (58) over the noninteracting density of states $N^0(\omega) = -\mathrm{Im}\, g_r^0(\omega)/\pi$, but for $2\Omega < eV < 13\Omega$ nearly all the noninteracting spectral weight is included. Consequently, the approximation I_a, and thus I, is suppressed, compared to I_0. This suppression disappears at $eV = 4\Omega$, resulting in a step of approximate height $0.5g$ times the noninteracting current. The prefactor, $0.5g$, is the approximate fraction of spectral weight of $N(\omega)$ in the upper satellite peak, because the resonant level is half occupied. We note that this prefactor depends on the filling

condition of the resonant level, and the step corresponds to that predicted at the bias $eV = 2(\Omega + (E_r - \mu)) \approx 4\Omega$ in Ref. [4].

(2) The shoulder in the interacting current arises from electrons tunneling inelastically via phonon emission. In the noninteracting case there is only a very small current, because E_r is below ϕ_L. For the interacting case, if $E_r + \Omega > \phi_L$, an electron can enter the resonant site from the left at energy $E_r + \Omega$, decay via emission of a phonon to energy E_r, and subsequently tunnel to the right lead. The large density of states at energy E_r therefore leads to an enhanced inelastic tunneling, which persists until the lower band-edge ϕ_L of the left lead is pushed above $E_r + \Omega$ at $eV \approx 15\Omega$.

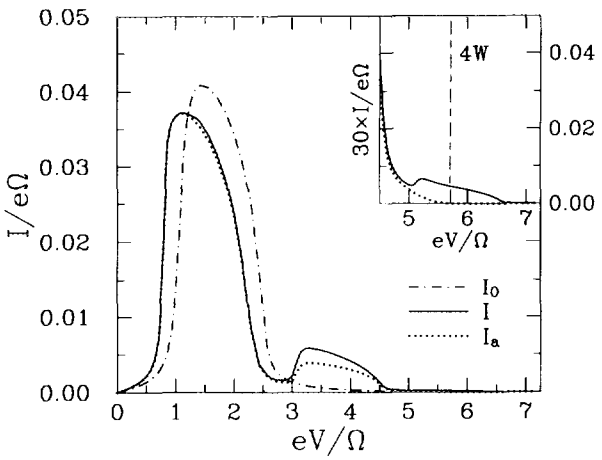

FIG. 7. The I-V characteristic in a low-doping case, where the depth of the Fermi sea $\mu + 2W$ is comparable to Ω, and the bandwidth is reduced to $4W \approx 6\Omega$. Again the escape rates are equal in equilibrium; the parameters are listed in Table I. In the region of large resonant currents, $\Omega < eV < 2.5\Omega$, the escape rates can be regarded as energy independent, and the term I_a (dotted curve) is still a very good approximation to interacting current I (solid curve), but the correction $I_c = I - I_a$ is important in the valley region, at biases $eV > 2.5\Omega$. Differences from the high-doping case are: (1) The noninteracting current I_0 (dash-dotted curve) differ significantly from the interacting current I (solid curve), because the spectral weight of $N(\omega) = -\text{Im}\, g_r(\omega)/\pi$ is always only partially included in the integral Eq. (63) proportional to I_a. The peak noninteracting current is larger than the peak noninteracting current, because more weight of the noninteracting density of state is included. (2) In the valley region, the current shows a satellite peak not just a shoulder, at biases $3\Omega < eV < 4.5\Omega$, because when ϕ_L is pushed above E_r, at bias $eV \approx 2.5\Omega$, μ_L is not yet above $E_r + \Omega$. Not until $\mu_L > E_r + \Omega$, at bias $eV \approx 3\Omega$, can electrons tunnel inelastically. (3) The correction term $I_c = I - I_a$ is of greater relative significance in the valley region. The energy dependence of $\Gamma_L(\omega)$ can not be neglected at biases where the satellite peak is observed, because $\Gamma_L(E_r)$ is zero, whereas $\Gamma_L(E_r)$ is nonzero. The correction term I_c therefore becomes significant in the valley region. I_c is more important in the valley region in this case compared to the high-doping case, because I_c depends on the ratio $\Gamma_L(E_r + \Omega)/\Gamma_R(E_r + \Omega)$ at the shoulder/satellite peak, and this ratio is made larger by the reduced bandwidth. Consider finally the insert, which shows the current I (solid curve), and the approximation I_a (dotted curve) scaled by a factor of 30, in the region of extreme bias, $eV > 4W \approx 6\Omega$. Here the left and right bands are not aligned and $I_a \equiv 0$, but there is still a nonvanishing current carried exclusively by $I_c \neq 0$.

Low-Doping Case. The I-V characteristic in the low-doping case, shown in Fig. 7, is qualitatively different from the I-V characteristic in the high-doping case. To study a low-doping case, we have reduced the thickness of the equilibrium Fermi sea to $\mu + 2W \approx 0.7\Omega$. We have also reduced the bandwidth to $4W \approx 6\Omega$, which, as explained below, increases the differences between the noninteracting and interacting current in the valley region. The escape rates are equal in equilibrium; the parameters are listed in Table I. Despite the reduced bandwidth, the escape rates $\Gamma_L(\omega)$ and $\Gamma_R(\omega)$ can still be regarded as energy independent in the region of large resonant currents $\Omega < eV < 2.5\Omega$. Thus the density-of-states term I_a (dotted curve) is still an excellent approximation to the interacting current (solid curve), for biases $\Omega < eV < 2.5\Omega$. As in the high-doping case the correction term $I_c = I - I_a$ only becomes significant in the valley region at biases $eV > 2.5\Omega$.

The reduced depth of the Fermi sea, $\mu + 2W \approx 0.7\Omega$, and the reduced bandwidth $4W \approx 6\Omega$ results in the following differences from the high-doping case: (1) The interacting current I (solid curve) is significantly different from the noninteracting current I_0 (dash-dotted curve) everywhere, even in the region of large resonant current. (2) In the valley region the shoulder is replaced by a clearly observable satellite peak in the interacting current at biases $3\Omega < eV < 4.5\Omega$. (3) While I_a (dotted curve) is still a very good approximation to I (solid curve) in the region of large resonant currents, the correction $I_c = I - I_a$ becomes comparable to I_a at biases where the satellite peak in I is observed. These differences between the high-doping and low-doping cases are discussed below.

(1) In this low-doping case the spectral weight of $N(\omega) = -\mathrm{Im}\, g_r(\omega)/\pi$ is only partially included in the integral Eq. (60) yielding I_a at all biases, because Ω is larger than the depth of the Fermi sea $\mu + 2W$. When evaluating the noninteracting current, at the bias of peak value, more of the noninteracting spectral weight is included. The peak value of the noninteracting current is therefore larger than the peak value of the interacting current.

(2) In the valley region, where $E_r < \phi_L$, the current shows a clearly distinctive satellite peak because an electron can enter at $E_r + \Omega$, emit a phonon, and thereby exploit the large density of states at E_r. A satellite peak, not just a shoulder, is observed because at the bias where ϕ_L is pushed above E_r, the Fermi surface of the left lead, μ_L, is not yet above $E_r + \Omega$. Not until $\mu_L > E_r + \Omega$ can electrons use the high density of states at E_r to tunnel inelastically.

(3) As in the high-doping case the correction $I_c \equiv I - I_a$ to I_a is of relative importance in the region where the shoulder/satellite peak in the interacting current I is observed. In that region the energy dependence of $\Gamma_L(\omega)$ *cannot* be neglected, because $\Gamma_L(E_r)$ is identically zero, but $\Gamma_L(E_r + \Omega)$ is nonzero. The net scattering-out rate $\sigma_>(\omega)\, g_<(\omega) - \sigma_<(\omega)\, g_>(\omega)$ has a positive (negative) peak at $\omega = E_r + \Omega$ ($\omega = E_r$) from electrons scattering out (in). The prefactor in $I_c(\omega)$ (see Eq. (62)) to the net scattering-out rate is $-\frac{1}{2}$ at $\omega = E_r$, since $\Gamma_L(E_r)$ is zero, but it has a smaller negative value at $\omega = E_r + \Omega$ because $\Gamma_L(E_r + \Omega)$ is finite. Thus we obtain a positive peak in $I_c(\omega)$ at $\omega = E_r$, which is only partially offset by a smaller negative peak

at $\omega = E_r + \Omega$. Decreasing the ratio $4W/\Omega$ makes $\Gamma_L(E_r+\Omega)/\Gamma_R(E_r+\Omega)$ larger when $E_r < \phi_L$, and the correction term I_c is therefore relatively more important in the low-doping case than in the high-doping case.

Finally consider the insert of Fig. 7, which shows the interacting current I (solid curve) and the density-of-states term I_a (dotted curve) enlarged in the region of extreme biases, $eV > 4W \approx 6\Omega$. In this region ϕ_L is above the *upper* band-edge of the right lead, but there is still a small but nonzero current. This current is carried exclusively by I_c because $T_a(\omega)$ is zero at all energies and, in the limit of extreme biases, the density-of-states term I_a thus fails to describe the small but nonvanishing current resulting from inelastic tunneling.

III.C. *Discussion of the Current Terms I_a and I_c*

In Section III.A we expressed the current $I = (I_L + I_R)/2$ as a sum $I = I_a + I_c$, where the expression Eq. (60) for the density-of-states term I_a is very similar in form to the expression Eq. (58) for the noninteracting current. Here we discuss that separation further. The noninteracting current is given as an integral (see Eq. (58)) from μ_R to μ_L over the noninteracting transmission coefficient $T_0(\omega)$ expressed in Eq. (57). The density-of-states term I_a is given by a similar integral Eq. (60) from μ_R to μ_L of

$$T_a(\omega) = \frac{2\Gamma_L(\omega)\,\Gamma_R(\omega)}{\Gamma_L(\omega)+\Gamma_R(\omega)}\,2\pi N(\omega). \tag{64}$$

Because the correction term I_c can often be neglected, it is tempting to view $T_a(\omega)$ as a generalization of the noninteracting transmission coefficient, $T_0(\omega)$. However, to interpret $T_a(\omega)$ as an effective interacting transmission coefficient, it must describe the current density per unit energy. We note that the current density at the resonant site is given by

$$\frac{I_L(\omega)+I_R(\omega)}{2} = T_a(\omega)[f_L(\omega) - f_R(\omega)] + I_c(\omega), \tag{65}$$

and we discuss below the problems with the interpretation of $T_a(\omega)$ as an transmission coefficient for the interacting problem.

A key point is that while $I_c = \int I_c(\omega)\,d\omega/\pi$ does vanish when the escape rates can be treated as constants, $\Gamma_{L/R} \equiv \Gamma_{L/R}(\omega)$, the function $I_c(\omega)$ (see Eq. (62)) vanishes only when Γ_L is equal to Γ_R. For constant escape rates the energy dependence of $I_c(\omega)$ is given by the net scattering-out rate, $\sigma_>(\omega)\,g_<(\omega) - \sigma_<(\omega)\,g_>(\omega)$, which can have a rich energy dependence, even if its integral must vanish. Figure 8 shows the contributions $T_a(\omega)$ and $I_c(\omega)$ at a fixed bias $eV = 6\Omega$ (indicated by the arrow in Fig. 6) for two different ratios of the escape rates. The contribution $T_a(\omega)$ is integrated from $\mu_L \approx -4\Omega$ to $\mu_R \approx 2\Omega$, whereas $I_c(\omega)$ is integrated over all the energies. The dotted curves show $T_a(\omega)$ and $I_c(\omega)$ when the escape rates are approximately equal, $\Gamma_L(\omega) \approx \Gamma_R(\omega)$, with parameters of the high-doping case as in

Fig. 6. Then $I_c(\omega)$ is approximately zero, and it might appear reasonable to interpret $T_a(\omega)$ as an *effective* probability for tunneling of electrons at energy ω. However, when $\Gamma_L(\omega)$ is much less than $\Gamma_R(\omega)$ with other parameters unchanged (solid curve), $I_c(\omega)$ has a significant energy dependence and at some energies $I_c(\omega)$ can be comparable or even larger than $T_a(\omega)$. The same is true for the opposite limit, $\Gamma_L(\omega) \gg \Gamma_R(\omega)$. Thus in general there is significant energy dependence of the current density of the resonant level, Eq. (65), which is not included in $T_a(\omega)$.

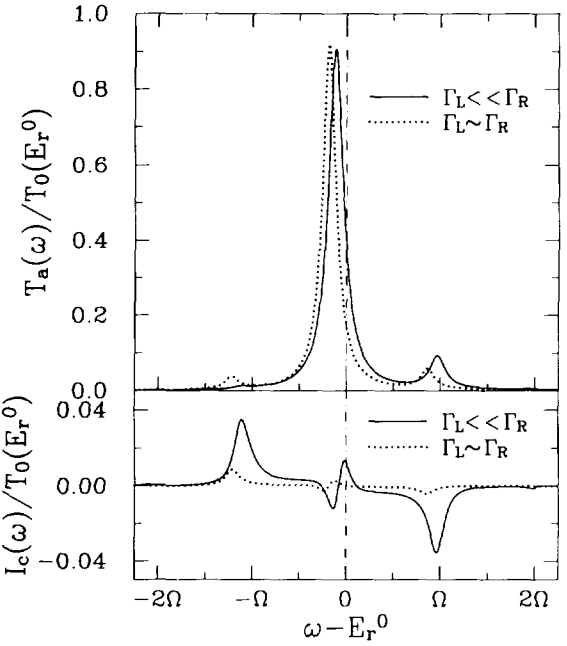

FIG. 8. The separation of the current into a density-of-states term I_a and a correction I_c in a high-doping calculation at bias $eV = 6\Omega$ for different ratios of $\Gamma_L(\omega)$ to $\Gamma_R(\omega)$. The dotted curves displays the case when $\Gamma_L(\omega) \approx \Gamma_R(\omega)$ ($W_L^2/W = W_R^2/W = 0.05\Omega$; the same situation as in Fig. 6 at bias indicated by arrow), and the resonant level is half occupied. The solid curves show the case when $\Gamma_L(\omega) \ll \Gamma_R(\omega)$ ($W_L^2/W = 0.01\Omega$, $W_R^2/W = 0.09\Omega$; the parameters otherwise are identical), and the system is in regime **A**. All the curves are scaled by the peak noninteracting transmission coefficient, $T_0(E_r^0) = 4\Gamma_L(E_r^0)\,\Gamma_R(E_r^0)/(\Gamma_L(E_r^0) + \Gamma_R(E_r^0))^2$. The density-of-states term I_a is given by an integral from $\mu_R - E_r^0 \approx -4\Omega$ to $\mu_L - E_r^0 \approx 2\Omega$ of $T_a(\omega)$ (see Eq. (64)) shown in the upper panel. The escape rates $\Gamma_L(\omega)$ and $\Gamma_R(\omega)$ depend only weakly on energy for $eV \approx 6\Omega$ at energies $|\omega - E_r| < 2\Omega$ and $T_a(\omega) \propto N(\omega) = -\mathrm{Im}\, g_r(\omega)/\pi$. Thus $T_a(\omega)$ reflects the behavior of the density of states $N(\omega)$: small (intermediate) polaron shift $E_r - E_r^0 \approx -0.1\Omega$ (-1.2Ω), and one (two) satellite peak(s) at $E_r + (\pm)\Omega$ for $\Gamma_L(\omega) \ll \Gamma_R(\omega)$ ($\Gamma_L(\omega) \approx \Gamma_R(\omega)$). The correction-term I_c is given by an integral over $I_c(\omega)$ (see Eq. (62)) shown in the lower panel. The contribution $I_c(\omega)$ is small for $\Gamma_L(\omega) \approx \Gamma_R(\omega)$ (dotted curve), but have significant energy-dependence for $\Gamma_L(\omega) \ll \Gamma_R(\omega)$ (solid curve) and for $\Gamma_L(\omega) \gg \Gamma_R(\omega)$ (regime **B**, not shown), even if $I_c = \int I_c(\omega)\, d\omega/\pi \approx 0$. Thus $T_a(\omega)$ does not in general correctly describe the current density of the resonant site, $T_a(\omega)(f_L(\omega) - f_R(\omega)) + I_c(\omega)$, and $T_a(\omega)$ cannot be interpreted as an effective transmission coefficient for the interacting problem.

A second problem with the interpretation of $T_a(\omega)$ as an effective transmission coefficient is to identify to what electrons the energy ω corresponds. When we are in regime **A**, where the satellite peak is at $E_r + \Omega$ above the main peak, that satellite peak results from electrons scattering *out* from energy $\omega \approx E_r + \Omega$ (see Section II.D). However, when we are in regime **B**, and the resonant-site density of states have a satellite peak at $E_r - \Omega$, that peak is due to electrons scattering *in* at energies $\omega \approx E_r - \Omega$.

III.D. *Elastic and Inelastic Current Contributions*

Another possible separation of the current density is into an elastic and inelastic contribution. We expect some electrons to tunnel elastically, i.e., without change of energy, but other electrons will experience inelastic scattering while at the resonant level. A separation of the current density into the elastic and inelastic contributions, which are sometimes also called the coherent and incoherent contributions, can provide some intuitive understanding of the scattering. In an earlier paper [32] we made such a separation into two contributions which we interpreted as the elastic and inelastic contribution to the current density $(I_L(\omega) + I_R(\omega))/2$ of the resonant site. As discussed in the previous subsections, working with the current density of the resonant site, $(I_L(\omega) + I_R(\omega))/2$, is useful because the current $I = (I_L + I_R)/2$ is then approximated by an integral over $T_a(\omega) \propto N(\omega)$, where the correction I_c typically vanishes. When discussing the effect of the interaction upon the total current, which was the primary motivation in Ref. [32], the current density of the resonant site, $(I_L(\omega) + I_R(\omega))/2$, is thus the natural starting point. For understanding other properties of the system, it is more helpful to retain the information contained in the current densities of the left and right leads, $I_L(\omega)$ and $I_R(\omega)$. Below we separate these current densities into an elastic and inelastic contribution, following the principles introduced in Ref. [32]. These elastic and inelastic current contributions have simple interpretations, which are discussed below. They show very directly the effects of the inelastic scattering and are useful in studying the energy transfer from the electrons to the phonon system. A similar separation and interpretation of the current has also recently been discussed by Lake *et al.* [33].

To make a separation into elastic and inelastic contributions, we insert the results for $2\pi N(\omega) = -2 \operatorname{Im} g_r(\omega)$ (see Eq. (22)) and for $g_<(\omega)$ (Eq. 21)) into the current densities of the left and right leads

$$I_L(\omega) = 2\Gamma_L(\omega)\,|g_r(\omega)|^2\,[2\Gamma_R(\omega)(f_L(\omega) - f_R(\omega))] + 2\Gamma_L(\omega)\,|g_r(\omega)|^2\,[f_L(\omega)\,\sigma_>(\omega) - (1 - f_L(\omega))\,\sigma_<(\omega)], \tag{66}$$

$$I_R(\omega) = 2\Gamma_R(\omega)\,|g_r(\omega)|^2\,[2\Gamma_L(\omega)(f_L(\omega) - f_R(\omega))] + 2\Gamma_R(\omega)\,|g_r(\omega)|^2\,[(1 - f_R(\omega))\,\sigma_<(\omega) - f_R(\omega)\,\sigma_>(\omega)]. \tag{67}$$

The underlying principle used in the separation into elastic and inelastic contributions rest upon the *explicit* presence of a less-than ($\sigma_<(\omega)$), or a greater-than self-energy ($\sigma_>(\omega)$) in the above expressions for the current densities [32]. Because the

terms with an explicit presence of $\sigma_>(\omega)$ or $\sigma_<(\omega)$ corresponds to contributions from electrons which are scattered out or in, we keep only the first terms of Eqs. (66) and (67) in the elastic contributions,

$$I_{elL}(\omega) = I_{elR}(\omega) \equiv T_{el}(\omega)[f_L(\omega) - f_R(\omega)], \tag{68}$$

where we have introduced

$$\begin{aligned} T_{el}(\omega) &= 4\Gamma_L(\omega)\,\Gamma_R(\omega)\,|g_r(\omega)|^2 \\ &= \frac{2\Gamma_L(\omega)\,\Gamma_R(\omega)}{\Gamma_L(\omega)+\Gamma_R(\omega)}\,|g_r(\omega)|^2\,[2\Gamma_L(\omega)+2\Gamma_R(\omega)]. \end{aligned} \tag{69}$$

Note that $T_{el}(\omega)$ is formally very similar to $T_0(\omega)$ and $T_a(\omega)$. We interpret $T_{el}(\omega)$ as the probability that an electron at ω tunnels through the system *elastically*, i.e., without a change in energy [32]. As expected the elastic contribution is the same for both leads. Note, however, that $T_{el}(\omega)$ implicitly, via $|g_r(\omega)|^2$, includes scattering processes.

The inelastic current contribution consist of the terms of Eqs. (66) and (67) with an explicit presence of a less-than or a greater-than self-energy

$$I_{inL}(\omega) = 2\Gamma_L(\omega)\,f_L(\omega)\,|g_r(\omega)|^2\,\sigma_>(\omega) - 2\Gamma_L(\omega)[1-f_L(\omega)]\,|g_r(\omega)|^2\,\sigma_<(\omega), \tag{70}$$

$$I_{inR}(\omega) = 2\Gamma_R(\omega)[1-f_R(\omega)]\,|g_r(\omega)|^2\,\sigma_<(\omega) - 2\Gamma_R(\omega)\,f_R(\omega)\,|g_r(\omega)|^2\,\sigma_>(\omega). \tag{71}$$

The current densities of the left (right) lead is thus given by

$$I_{L(R)}(\omega) = T_{el}(\omega)[f_L(\omega) - f_R(\omega)] + I_{inL(R)}(\omega), \tag{72}$$

and by current conservation, we have

$$\int_{-\infty}^{\infty} \frac{d\omega}{2\pi}\,[I_{inL}(\omega) - I_{inR}(\omega)] = 0. \tag{73}$$

Because of Eq. (72) we see that the *change* in the current distribution before and after the electron–phonon interaction at the resonant site is given by comparing $I_{inL}(\omega)$ and $I_{inR}(\omega)$. These inelastic current contributions therefore provide information about the energy transfer due to inelastic scattering at the resonant level.

To simplify the discussion of $I_{inL}(\omega)$ and $I_{inR}(\omega)$ we restrict ourselves to the zero-temperature case. Here we find that the second term of Eq. (70) vanishes,

$$-2\Gamma_L(\omega)[1-f_L(\omega)]\,|g_r(\omega)|^2\,\sigma_<(\omega) \equiv 0, \tag{74}$$

because $\sigma_<(\omega) \propto g_<(\omega+\Omega)$ is zero for $\omega > \mu_L - \Omega$, whereas $[1\text{-}f_L(\omega)]$ is zero for $\omega < \mu_L$. Thus none of the electrons which are scattered-in (from a higher energy) return to the left, and $I_{inL}(\omega)$ reduces to

$$I_{inL}(\omega) = 2\Gamma_L(\omega)\,f_L(\omega)\,|g_r(\omega)|^2\,\sigma_>(\omega). \tag{75}$$

Similarly, the second term of Eq. (71) vanishes,

$$-2\Gamma_R(\omega) f_R(\omega) |g_r(\omega)|^2 \sigma_>(\omega) \equiv 0, \tag{76}$$

because $\sigma_>(\omega)$ is zero for $\omega < \mu_R + \Omega$, but $f_R(\omega)$ is zero for $\omega > \mu_R$. Consequently no electrons enter from the right and are scattered out, and $I_{inR}(\omega)$ reduces to

$$I_{inR}(\omega) = 2\Gamma_R(\omega)[1 - f_R(\omega)] |g_r(\omega)|^2 \sigma_<(\omega). \tag{77}$$

Based on Eqs. (75) and (77) we now interpret:

(1) $I_{inL}(\omega)$ as the density of electrons *entering* the resonance from the left at energy ω, but scatter out to lower energy $\omega - \Omega$. Because of Eq. (76), we see that all electrons which are scattered out contribute to $I_{inL}(\omega)$.

(2) $I_{inR}(\omega)$ as the current density of electrons that scatter in from higher energy $\omega + \Omega$, and *leave* the resonant level for the right lead at energy ω. Because of Eq. (74) we find that all electrons that are scattered in contribute to $I_{inR}(\omega)$.

The upper panel of Fig. 9 shows the elastic contribution $T_{el}(\omega)$ (solid curve), compared to the noninteracting transmission coefficient $T_0(\omega)$ (dash-dotted curve), in the case of $\Gamma_L(\omega) \ll \Gamma_R(\omega)$ at bias $eV = 6\Omega$ (same situation as shown by the solid curves in Fig. 8). The resonant level is still within both bands, and the energy dependence of $\Gamma_L(\omega)$ and $\Gamma_R(\omega)$ can be ignored. At this bias, $T_{el}(\omega)$ for the interacting current, and $T_0(\omega)$ in the noninteracting case, must be integrated from $\mu_R \approx -4\Omega$ to $\mu_L \approx 2\Omega$. The peak of the elastic contribution $T_{el}(\omega)$ at E_r, is shifted from the peak of the noninteracting transmission coefficient $T_0(\omega)$ at E_r^0 by approximately $g\Omega = 0.1\Omega$. That is expected because $\Gamma_L(\omega) \ll \Gamma_R(\omega)$ and the system is in regime **A**. However, $T_{el}(\omega)$ is not merely a (shifted) damped version of $T_0(\omega)$. As shown more clearly in the insert, $T_{el}(\omega)$ exhibit a resonant structure at $E_r + \Omega$. It is first smaller than $T_0(\omega)$ for $\omega < E_r + \Omega$, but runs through a resonance and becomes larger than $T_0(\omega)$ for $\omega > E_r + \Omega$. This behavior corresponds to a Fano line shape [55] of positive q-value. In the same situation, but with $\Gamma_L(\omega) \gg \Gamma_R(\omega)$ (not shown), a similar structure in $T_{el}(\omega)$ is observed at $\omega \approx E_r - \Omega$. In that case $T_{el}(\omega)$ is first greater than $T_0(\omega)$ for $\omega < E_r - \Omega$, but becomes smaller than $T_0(\omega)$ for $\omega > E_r - \Omega$ corresponding to a Fano line shape of negative q-value. In the case of $\Gamma_L(\omega) \approx \Gamma_R(\omega)$ (also not shown), two such structures are observed in $T_{el}(\omega)$, one at $E_r - \Omega$ and the other at $E_r + \Omega$.

The middle panel of Fig. 9 shows the inelastic current contribution for the left lead, $I_{inL}(\omega)$, while the lower panel of Fig. 9 shows $I_{inR}(\omega)$. Both contributions are scaled by the peak noninteracting transmission coefficient, $T_0(E_r^0) = 4\Gamma_L\Gamma_R/\Gamma^2$, where $\Gamma_{L/R} \equiv \Gamma_{L/R}(E_r^0)$. $I_{inL}(\omega)$ ($I_{inR}(\omega)$) is the contribution from electrons scattering-*out* from energy ω (scattering-*in* at energy ω). $I_{inL}(\omega)$ therefore has a peak at $E_r + \Omega$ because of the large density of final states at E_r for *scattering-out* processes and a peak at E_r because of the large density of initial states. Similarly, $I_{inR}(\omega)$ has a peak at E_r because of the large density of final states at E_r for *scattering-in* processes and at $E_r - \Omega$ because of the large density initial states.

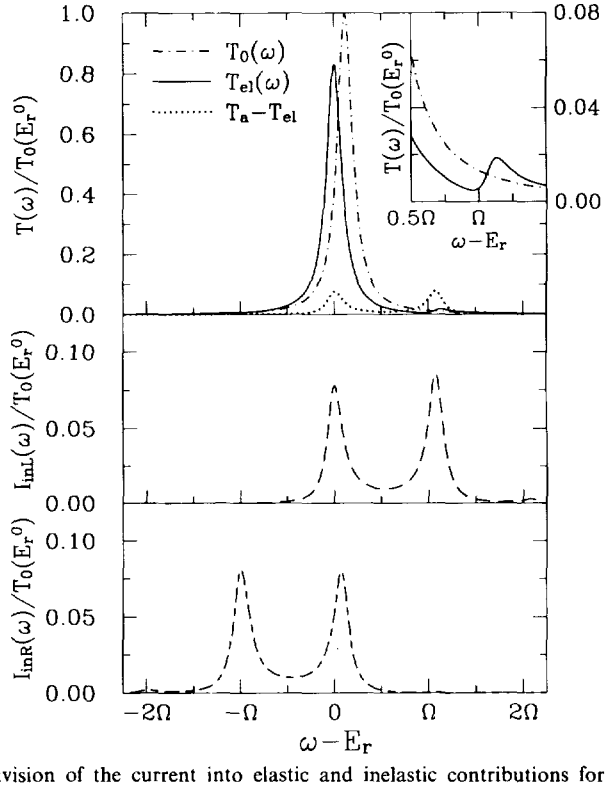

FIG. 9. The division of the current into elastic and inelastic contributions for the same situation shown by the solid curves in Fig. 8. The *upper* panel shows the noninteracting transmission coefficient $T_0(\omega)$ (dash-dotted curve) (see Eq. (57)), and the interacting elastic contribution $T_{el}(\omega)$ (solid curve) (see Eq. (69)). Both must be integrated from $\mu_R - E_r \approx -4\Omega$ to $\mu_L - E_r \approx 2\Omega$. The *upper* panel also shows $T_a(\omega) - T_{el}(\omega)$ (dotted curve). The current density in the left and right leads is $T_{el}(\omega)[f_L(\omega) - f_R(\omega)] + I_{inL}(\omega)$ and $T_{el}(\omega)[f_L(\omega) - f_R(\omega)] + I_{inR}(\omega)$, respectively. $I_{inL}(\omega)$ (dashed curve in the *middle* panel) (see Eq. (70)) can be interpreted as the density of electrons entering the resonance at energy ω from the left lead and are scattered out to lower energy $\omega - \Omega$. It therefore has a peak at $E_r + \Omega$ (large density of final states) and at E_r (large density of initial states). $I_{inR}(\omega)$ (alternating long/short dashed curve in *lower* panel) (see Eq. (71)) can be interpreted as the density of electrons scattering in at energy ω from energy $\omega + \Omega$ and *leave* for the right. It therefore has a peak at E_r (large density of final states) and at $E_r - \Omega$ (large density of initial states). The insert shows the elastic contribution $T_{el}(\omega)$ (solid curve), and the noninteracting transmission coefficient $T_0(\omega)$ (dash-dotted curve) around $E_r + \Omega$, where the density of state $N(\omega) = -\text{Im}\, g_r(\omega)/\pi$ has a satellite peak because the system is in regime A. Note that $T_{el}(\omega)$ is first smaller than $T_0(\omega)$ for $\omega - E_r < \Omega$. At $\omega - E_r \approx \Omega$ it runs through a resonance and becomes larger than $T_0(\omega)$.

The structure in $I_{inL}(\omega - E_r)/T_0(E_r^0)$ and $I_{inR}(\omega - E_r)/T_0(E_r^0)$ is independent of the filling condition when the escape rates are constant, $\Gamma_{L/R} \equiv \Gamma_{L/R}(\omega = E_r)$, and we are in a high-bias limit with $f_R(\omega) \approx 0$, $f_L(\omega) \approx 1$, and $f_{eff}(\omega) \approx \Gamma_L/\Gamma$, where $\Gamma = \Gamma_L + \Gamma_R$. For the case displayed in Fig. 9 these conditions are met even though $\mu_L - E_r \approx 2\Omega$ and $E_r - \mu_R \approx 4\Omega$. Figure 9 thus shows the qualitative form of $I_{inL}(\omega - E_r)/T_0(E_r^0)$ and of $I_{inR}(\omega - E_r)/T_0(E_r^0)$ for general filling conditions. To see

this analytically, we examine $I_{\text{inL/R}}(\omega)$ to first order in g for constant escape rates. We denote these estimates for the inelastic contributions $I^{(1)}_{\text{inL/R}}(\omega)$.

The key observation is that the scattering-out rate (Eq. (55)) and scattering-in rate (Eq. (56)) scales with $T_0(E_r^0)$, but does not otherwise depend on Γ_L/Γ_R to first order in g, when $f_{\text{eff}}(\omega)$ can be approximated by Γ_L/Γ for energies $|\omega - E_r| < 2\Omega$. In this case the first-order estimates for the non-equilibrium less-than and greater-than self-energies are

$$\sigma^{(1)}_<(\omega) \approx \frac{2M^2\Gamma_L}{(\omega + \Omega - E_r^0)^2 + \Gamma^2}, \tag{78}$$

$$\sigma^{(1)}_>(\omega) \approx \frac{2M^2\Gamma_R}{(\omega - \Omega - E_r^0)^2 + \Gamma^2}, \tag{79}$$

and the first-order expressions for the inelastic current contributions become

$$\begin{aligned} I^{(1)}_{\text{inL}}(\omega) &= 2\Gamma_L f_L(\omega)\,|g_r^0(\omega)|^2\,\sigma^{(1)}_>(\omega) \\ &\approx \frac{4g\Omega^2\Gamma_L\Gamma_R}{[(\omega - E_r^0)^2 + \Gamma^2][\omega - \Omega - E_r^0)^2 + \Gamma^2]}, \end{aligned} \tag{80}$$

$$\begin{aligned} I^{(1)}_{\text{inR}}(\omega) &= 2\Gamma_R[1 - f_R(\omega)]\,|g_r^0(\omega)|^2\,\sigma^{(1)}_<(\omega) \\ &\approx \frac{4g\Omega^2\Gamma_L\Gamma_R}{[(\omega - E_r^0)^2 + \Gamma^2][(\omega + \Omega - E_r^0)^2 + \Gamma^2]}. \end{aligned} \tag{81}$$

Thus $I^{(1)}_{\text{inL}}(\omega)$ ($I^{(1)}_{\text{inR}}(\omega)$) has two peaks, one at $E_r^0 + \Omega$ (E_r^0) and one at E_r^0 ($E_r^0 - \Omega$). The ratios $I^{(1)}_{\text{inL}}(\omega)/T_0(E_r^0)$ and $I^{(1)}_{\text{inR}}(\omega)/T_0(E_r^0)$ at the two peaks are

$$I^{(1)}_{\text{inL}}(E_r^0 + \Omega)/T_0(E_r^0) = I^{(1)}_{\text{inL}}(E_r^0)/T_0(E_r^0) = g\frac{\Omega^2}{\Omega^2 + \Gamma^2}, \tag{82}$$

$$I^{(1)}_{\text{inR}}(E_r^0)/T_0(E_r^0) = I^{(1)}_{\text{inR}}(E_r^0 - \Omega)/T_0(E_r^0) = g\frac{\Omega^2}{\Omega^2 + \Gamma^2}. \tag{83}$$

Note that the filling condition, set by Γ_L/Γ_R, does not enter in either the position of the peaks, or in the estimates Eqs. (82) and (83) for the scaled peak heights. In the self-consistent case the resonant level will, of course, depend on the filling condition, and this will result in a shift of the peaks of $I_{\text{inL/R}}(\omega)$. However, the *qualitative* behavior of $I_{\text{inL/R}}(\omega - E_r)/T_0(E_r^0)$ is independent of the filling condition, when the escape rates can be treated as energy independent and when in a high-bias limit, where $f_{\text{eff}}(\omega) \approx \Gamma_L/\Gamma$ for energies $|\omega - E_r| < 2\Omega$.

We note that the elastic contribution $T_{\text{el}}(\omega - E_r)$ scales with the same overall factor, $T_0(E_r^0)$, under these typical conditions (see Eq. (69)). Hence, the elastic, $T_{\text{el}}(\omega - E_r)$, and inelastic contribution, $I_{\text{inL/R}}(\omega - E_r)$, to the total current density $I_{\text{L/R}}(\omega - E_r)$ have the same *relative* weight at all filling conditions. The shape of the inelastic contribution $I_{\text{inL/R}}(\omega - E_r)$ is, furthermore, also independent of the filling

condition, unlike the shape of the elastic contribution, where a resonant structure is observed at $\omega = E_r + \Omega$ when the system is in regime **A**, but at $\omega = E_r - \Omega$ when the system is in regime **B**.

IV. Conclusion

In this paper we used nonequilibrium quantum-statistical mechanics to study the equilibrium behavior and the nonlinear transport in a one-dimensional resonant-tunneling system with an electron–phonon interaction at zero temperature. The formal derivations can easily be generalized to three dimensions, but the corresponding numerical calculations are more involved. The purpose of our one-dimensional model calculation has not been a quantitative description of the standard semiconductor heterostructure resonant tunneling devices (for which a three-dimensional treatment is needed). Instead, we have attempted to illustrate some qualitative features of resonant tunneling with an electron–phonon interaction. In particular, our calculation is relevant to resonant tunneling through localized states, such as, for example, impurities located in a tunnel barrier.

We have assumed a weak electron–phonon coupling and have therefore treated the interaction in the self-consistent Born approximation, that is, to lowest order in the dimensionless coupling constant g. Because the system lacks translational invariance both the Fock-like *and* the Hartree-like diagrams must be retained.

By studying the equilibrium, resonant-site density of states we identified two qualitatively different regimes of the system, which depend on the filling condition of the resonant level. Regime **A** (empty resonant level) is characterized by a small negative polaron shift of the resonant level, $-g\Omega$, and by a satellite peak in the interacting resonant-site density of states *above* the main peak at E_r. Regime **B** (occupied resonant level) is characterized by a larger negative polaron shift, $-3g\Omega$, and by a satellite peak in the density of state *below* the resonant level. The inclusion of the Hartree diagram is essential to obtain the correct polaron shift in regime **B**. These two regimes also exist out of equilibrium at biases where a large resonant current flows. In that situation regime **A** (**B**) occurs when $\Gamma_L \ll \Gamma_R$ ($\Gamma_L \gg \Gamma_R$), where $\Gamma_{L/R}$ is the escape rate for tunneling from the resonant level to the left/right lead.

We studied the equilibrium polaron shift both numerically and analytically in the first Born approximation. We found a second perturbation parameter, $g\Gamma/\Omega$, in addition to the dimensionless coupling constant g. This new parameter must be small to study the equilibrium, zero-temperature polaron shift and to ensure that the interacting, resonant-site density of states remains positive to lowest order in g. This second perturbation parameter is important when the phonon frequency is larger than the escape rate, which is relevant for electrons interacting with optical phonon modes.

For the nonlinear transport, we verified explicitly that current is conserved, and we calculated the nonlinear I-V characteristics in both high-doping and low-doping

cases. The depth of the equilibrium Fermi sea is large compared to W in the high-doping case, while it is comparable to Ω in the low-doping case. In both cases we find that the density-of-states term, $I_a = \int_{\mu_R}^{\mu_L} T_a(\omega)\, d\omega/\pi$, is an excellent approximation to the interacting current at biases where a large resonant current flows. In the *high-doping* case the interacting current differs significantly from the noninteracting current in two places: (1) A small suppression of the interacting current, relative to the noninteracting current. This suppression arises because just after the onset of the large resonant current the upper satellite peak of the density of states is not yet included in the range of integration in I_a. (2) A shoulder in the interacting current is observed in the valley region. This shoulder results from electrons tunneling inelastically through the resonant level via phonon emission.

In the *low-doping* case with reduced thickness of the Fermi sea and reduced bandwidth, we observed the following differences from the high-doping case: (1) The interacting current differs significantly from the noninteracting current everywhere, since the integral I_a never includes the entire weight of the density of states. (2) A satellite peak, not just a shoulder, is observed in the valley region of the I-V characteristic. (3) The correction term $I_c \equiv I - I_a$ is of greater significance in the valley region, because the energy dependence of the escape rates are greater with the reduced bandwidth.

While the density-of-states term, $I_a = \int_{\mu_L}^{\mu_R} T_a(\omega)\, d\omega/\pi$, is typically the leading contribution to the current I, we have demonstrated that $T_a(\omega)$ cannot be interpreted as an effective transmission coefficient for the interacting problem. There is a correction term $I_c \equiv I - I_a$, which is significant in the valley region. Furthermore, the function $T_a(\omega)$ does not in general describe the current density per unit energy at the resonant level, even when I_a equals I.

Finally, the current densities for the left and right leads were separated into elastic and inelastic contributions. The elastic contribution to the current density of the leads are identical, while the inelastic contributions are different. We studied the elastic and inelastic contributions in a typical example, where we can assume that the escape rates are constant, and at a bias where $|\mu_{L/R} - E_r| \gg \Omega$. We found that the elastic contribution $T_{el}(\omega - E_r)$ depends on the filling condition of the resonant level: $T_{el}(\omega - E_r)$ has a peak at $\omega = E_r$ and a smaller resonant structure at energy $\omega = E_r + \Omega$ ($\omega = E_r - \Omega$), i.e., *above* (*below*) the main resonant peak in regime **A** (regime **B**). In the same example, we found that the ratio of the inelastic contribution $I_{inL(R)}(\omega - E_r)$ to the current density $I_{L(R)}(\omega - E_r)$ is independent of the filling condition and that $I_{inL}(\omega - E_r)(I_{inR}(\omega - E_r))$ has two peaks of equal height at $\omega = E_r + \Omega$ and at $\omega = E_r$ (at $\omega = E_r$ and at $\omega = E_r - \Omega$).

In summary we have found it essential to retain a Hartree-like electron–phonon self-energy diagram in this problem lacking translational invariance. We have identified qualitatively different regimes of the model, depending on the filling condition of the resonant level. These regimes have different polaron shifts, and we have found an important new perturbation parameter in the study of the equilibrium, zero-temperature polaron shift. We have provided a detailed understanding of when the noninteracting current is a poor predictor for the nonlinear, interacting

current-voltage characteristics, which we have calculated and explained in detail in typical cases. We have, furthermore, demonstrated that a natural candidate, $T_a(\omega)$, for an effective interacting transmission coefficient does not in general describe the current density per unit energy at the resonant level, and thus it fails. Finally, we have separated the current densities for the left and right leads into elastic and inelastic contributions, which we have studied in a typical example.

ACKNOWLEDGMENTS

We thank L. I. Glazman, A.-P. Jauho, W. E. Lawrence, M. Reizer, H. Smith, C. J. Stanton, and M. M. Steiner for useful discussions. This work was supported primarily by the U.S. Office of Naval Research and while the authors were at the Institute for Theoretical Physics in Santa Barbara, partially by NSF Grant No. PHY89-04035. One of the authors (P.H.) also acknowledges a licentiate stipend from the Danish Natural Science Research Foundation and the support of the Danish Research Academy.

REFERENCES

1. R. LANDAUER, *IBM J. Res. Dev.* **1** (1957), 233; *Phil. Mag.* **21** (1970), 863.
2. M. BÜTTIKER, *Phys. Rev. Lett.* **57** (1986), 1761.
3. M. BÜTTIKER, *Phys. Rev. B* **33** (1986), 3020.
4. L. I. GLAZMAN AND R. I. SHEKHTER, *Zh. Eksp. Teor. Fiz.* **94** (1988), 292; *Sov. Phys. JETP* **67** (1988), 163.
5. N. S. WINGREEN, K. W. JACOBSEN, AND J. W. WILKINS, *Phys. Rev. Lett.* **61** (1988), 1396.
6. L. I. GLAZMAN AND K. A. MATVEEV, *Zh. Eksp. Teor. Fiz.* **94** (1988), 332; *Sov. Phys. JETP* **67** (1988), 1276.
7. M. JONSON, *Phys. Rev. B* **39** (1989), 5924.
8. B. Y. GELFAND, S. SCHMITT-RINK, AND A. F. J. LEVI, *Phys. Rev. Lett.* **62** (1989), 1683.
9. W. CAI, T. F. ZHENG, P. HU, B. YUDANIN, AND M. LAX, *Phys. Rev. Lett.* **63** (1989), 418.
10. P. HYLDGAARD AND A.-P. JAUHO, *J. Phys.: Condens. Matter* **2** (1990), 8725.
11. J. A. STØVNENG, E. H. HAUGE, P. LIPAVSKY, AND V. SPIČKA, *Phys. Rev. B* **44** (1991), 595.
12. F. SOLS, *Ann. Phys. (N.Y)* **214** (1992), 386.
13. N. ZOU AND K. A. CHAO, *Phys. Rev. Lett.* **69** (1992), 3224.
14. C. CAROLI, R. COMBESCOT, P. NOZIERES, AND D. SAINT-JAMES, *J. Phys. C: Solid State Phys.* **4** (1971), 916; **5** (1972), 21.
15. R. TSU AND L. ESAKI, *Appl. Phys. Lett.* **22** (1973), 562.
16. W. R. FRENSLEY, *Phys. Rev. B* **36** (1987), 1570.
17. T. K. NG AND P. A. LEE, *Phys. Rev. Lett.* **61** (1988), 1768.
18. L. I. GLAZMAN AND M. E. RAIKH, *Pis'ma Zh. Eksp. Teor. Fiz.* **47** (1988), 378; *JETP Lett.* **47** (1988), 452.
19. H. A. FERTIG AND S. DAS SARMA, *Phys. Rev. B* **40** (1989), 7410.
20. J. LEO AND A. H. MACDONALD, *Phys. Rev. Lett.* **64** (1990), 817.
21. S. DATTA, *J. Phys.: Condens. Matter* **2** (1990), 8023.
22. F. A. BOUT AND K. L. JENSEN, *Phys. Rev. B* **42** (1990), 9429. While a formal description of the electron–phonon interaction in the self-consistent Born approximation is derived within the Wigner function approach, a relaxation-time approximation is used in practice.
23. Y. MEIR, N. S. WINGREEN, AND P. A. LEE, *Phys. Rev. Lett.* **66** (1991), 3048.
24. E. V. ANDA AND F. FLORES, *J. Phys.: Condens. Matter* **3** (1991), 9087.
25. S. HERSHFIELD, J. H. DAVIES, AND J. W. WILKINS, *Phys. Rev. Lett.* **67** (1991), 3720.

26. R. LAKE AND S. DATTA, *Phys. Rev. B* **45** (1992), 6670. The kinetic equation for the nonequilibrium Green functions are solved in the self-consistent Born approximation, neglecting, however, the real part of the self-energy.
27. E. RUNGE AND H. EHRENREICH, *Phys. Rev. B* **45** (1992), 9145; *Ann. Phys. (N.Y.)* **219** (1992), 55.
28. Y. MEIR AND N. S. WINGREEN, *Phys. Rev. Lett.* **68** (1992), 2512.
29. M. A. ALAM, R. A. MORRISEY, AND A. N. KHONDKER, *J. Appl. Phys.* **71** (1992), 3077.
30. S. HERSHFIELD, J. H. DAVIES, AND J. W. WILKINS, *Phys. Rev. B* **46** (1992), 7046.
31. F. W. J. HEKKING, Y. V. NAZAROV, AND G. SCHÖN, *Europhys. Lett.* **20** (1992), 255.
32. J. H. DAVIES, S. HERSHFIELD, P. HYLDGAARD, AND J. W. WILKINS, *Phys. Rev. B* **47** (1993), 4603.
33. R. LAKE, G. KLIMECK, AND S. DATTA, *Phys. Rev. B* **47** (1993), 6427.
34. Y. MEIR, N. S. WINGREEN, AND P. A. LEE, *Phys. Rev. Lett.* **70** (1993), 2601.
35. C. H. GREIN, E. RUNGE, AND H. EHRENREICH, *Phys. Rev. B* **47** (1993), 12590. The nonlinear current in the presence of electron–phonon interactions both in the quantum well and in the surrounding barriers is calculated within the first Born approximation. This paper does not discuss the self-energy shifts.
36. V. J. GOLDMAN, D. C. TSUI, AND J. E. CUNNINGHAM, *Phys. Rev. B* **36** (1987), 7635.
37. M. L. LEADBEATER, E. S. ALVES, L. EAVES, M. HENINI, O. H. HUGHES, A. CELESTE, J. C. PORTAL, G. HILL, AND M. A. PATE, *Phys. Rev. B* **39** (1989), 3438.
38. S. J. BENDING AND M. R. BEASLEY, *Phys. Rev. Lett.* **55** (1985), 324.
39. M. NAITO AND M. R. BEASLEY, *Phys. Rev. B* **35** (1987), 2548.
40. Y. XU, A. MATSUDA, AND M. R. BEASLEY, *Phys. Rev. B* **42** (1990), 1492.
41. S. GREGORY, *Phys. Rev. Lett.* **64** (1990), 689.
42. D. C. RALPH AND R. A. BUHRMAN, *Phys. Rev. Lett.* **69** (1992), 2118.
43. D. C. RALPH, K. S. RALLS, AND R. A. BUHRMAN, *Phys. Rev. Lett.* **70** (1993), 986.
44. L. L. CHANG, L. ESAKI, AND R. TSU, *Appl. Phys. Lett.* **24** (1974), 593.
45. L. P. KADANOFF AND G. BAYM, "Quantum Statistical Mechanics," Benjamin, New York, 1962.
46. L. V. KELDYSH, *Zh. Eksp. Teor. Fiz.* **47** (1964), 1515; *Sov. Phys. JETP* **20** (1965), 1018.
47. D. C. LANGRETH, "1975 NATO Advanced Study Institute on Linear and Nonlinear Electron Transport in Solids, Antwerpen, 1975," Vol. B17, pp. 3–32, Plenum, New York, 1976.
48. The Hartree diagram can be neglected in a system with translational invariance; see J. R. SCHRIEFFER, "Theory of Superconductivity," p. 145, Benjamin, New York, 1964.
49. The noninteracting transmission coefficient $T_0(\omega)$ is a Lorentzian peaked at the noninteracting resonant level, E_r^0. If the tunnel matrix elements are equal, $W_L = W_R$, and if the resonant level is still within both bands, $|E_r^0 - E_{L/R}| < 2W$, then the noninteracting resonant level is given by $E_r^0 = E_C/[1 - \frac{1}{2}(W_L/W)^2 - \frac{1}{2}(W_R/W)^2]$.
50. G. D. MAHAN, "Many-Particle Physics," pp. 269–310, Plenum, New York, 1981.
51. A. L. FETTER AND J. D. WALECKA, "Quantum Theory of Many-Particle Systems," pp. 121–127, McGraw–Hill, New York, 1971.
52. L. P. KADANOFF AND G. BAYM, "Quantum Statistical Mechanics," pp. 64–66, Benjamin, New York, 1962.
53. The *nonequilibrium* spectral function have qualitatively the same dependence on the filling condition as observed in Fig. 3 if we are at a high bias, where $|E_r - \mu_{L/R}| \gtrsim \Gamma = \Gamma_L + \Gamma_R$ (assuming, however, that $|E_r - \phi_{L/R}| \gtrsim \Gamma$). Regime **A** (**B**) then is obtained when $\Gamma_L \ll \Gamma_R$ ($\Gamma_L \gg \Gamma_R$), whereas the middle panel corresponds qualitatively to the case where $\Gamma_L = \Gamma_R$ and $f_{\text{eff}}(\omega) \equiv \frac{1}{2}$. However, the dramatic rise (drop) observed in the middle panel of Fig. 3 is absent in the high-bias nonequilibrium spectral function because, unlike for the corresponding equilibrium situation, there is no sudden onset (inhibition) of scattering-out (scattering-in) processes with increasing energy ω.
54. J. LINDHARD, *Kgl. Danske Videnskab. Selskab, Mat.-Fys. Medd.* **28** (8) (1954).
55. U. FANO, *Phys. Rev.* **124** (1961), 1866.